UNIVERSITAT POLITÈCNICA DE VALÈNCIA

UNIVERSITAT POLITÈCNICA DE VALÈNCIA

School of Industrial Engineering

Study of the use of deep eutectic solvents for the recovery of antimony by electrodeposition

Master's Thesis

Master's Degree in Industrial Engineering

AUTHOR: Gravensteyn, Cas

Tutor: Martí Calatayud, Manuel César

Experimental director: Santana Barros, Kayo

ACADEMIC YEAR: 2023/2024

ACKNOWLEDGMENTS

Over an intensive five-month period, this thesis on "Deep Eutectic Solvents" was accomplished. This journey has been both challenging and rewarding, and it would not have been possible without the support and guidance of several fantastic individuals to whom I am deeply grateful.

First and foremost, I would like to express my deepest gratitude to my supervisor, Professor Manuel César Martí Calatayud, for giving me the opportunity to work on this project. Your lightning-fast communication, invaluable feedback, expert advice, and continuous guidance have been my compass throughout this project.

I would also like to give a massive “Thank you!” to Kayo Santana Barros for your enthusiastic support throughout the project. Without your feedback, insightful comments, constructive suggestions, and continuous support in the lab, this thesis would not have been possible.

To my amazing parents, I can’t thank you enough for your steadfast support, not only during my Erasmus adventure but throughout all the preceding years. Your endless encouragement and belief in me have been my superpower.

Finally, a big thank you to everyone who has contributed directly or indirectly to this amazing experience and this thesis. I am truly grateful for each and every one of you.

Thank you all for making this journey an unforgettable and rewarding experience!

ABSTRACT

The European Commission issues an annual list of substances which are declared as Critical Raw Materials. This list includes metalloids, such as antimony, which are of special relevance for the industry and are at risk of supply.

Antimony, while present as an impurity in effluents generated by the copper industry, finds extensive application in various domains. It serves as a crucial component in liquid metal batteries and in the manufacturing of semiconductors, such as infrared detectors and diodes. Furthermore, it is widely used as a catalyst in the production of polyethylene terephthalate (PET) and as a flame retardant in cables, textiles, and plastics.

The recovery of antimony present in solid waste usually involves the use of highly concentrated inorganic acids to dissolve the metal. The selective separation of antimony from the resulting leachate or effluent can be conducted via electrodeposition.

This study focuses on utilizing an environmentally friendly alternative to classical solvents for the dissolution and recovery of antimony. The green solvent used in this research is the deep eutectic solvent, oxaline, which is composed of equimolar quantities of choline chloride and oxalic acid.

In this Master Thesis, the dissolution of antimony in oxaline and its subsequent recovery through electrodeposition were studied. First, the electrochemical characterization of oxaline and oxaline with dissolved antimony was conducted by means of cyclic voltammetry. This was followed by the identification of the most suitable operating conditions for antimony recovery from voltammograms obtained via linear sweep voltammetry.

In the final phase, galvanostatic and potentiostatic electrodeposition experiments were conducted using the previously determined current densities and potentials. The effectiveness of antimony recovery was evaluated through elemental analysis, specifically atomic absorption spectroscopy.

Keywords: Antimony, Green solvent, Deep Eutectic Solvent, Oxaline, Cyclic voltammetry, Electrodeposition, Critical Raw Material, Recovery of antimony.

RESUMEN

La Comisión Europea emite una lista anual de sustancias que se declaran como Materias Primas Críticas. Esta lista incluye metaloides, como el antimonio, que son de especial relevancia para la industria y están en riesgo de suministro.

El antimonio, aunque está presente como impureza en los efluentes generados por la industria del cobre, encuentra una amplia aplicación en diversos campos. Sirve como un componente crucial en baterías de metal líquido y en la fabricación de semiconductores, como detectores infrarrojos y diodos. Además, se utiliza ampliamente como catalizador en la producción de tereftalato de polietileno (PET) y como retardante de llama en cables, textiles y plásticos.

La recuperación de antimonio presente en residuos sólidos generalmente implica el uso de ácidos inorgánicos altamente concentrados para disolver el metal. La separación selectiva del antimonio del lixiviado o efluente resultante puede llevarse a cabo mediante electrodeposición.

Este estudio se centra en la utilización de una alternativa ecológica a los disolventes clásicos para la disolución y recuperación de antimonio. El disolvente verde utilizado en esta investigación es el disolvente eutéctico profundo, oxalina, que se compone de cantidades equimolares de cloruro de colina y ácido oxálico.

En esta Tesis de Máster, se estudió la disolución de antimonio en oxalina y su posterior recuperación mediante electrodeposición. Primero, se realizó la caracterización electroquímica de oxalina y oxalina con antimonio disuelto mediante voltamperometría cíclica. Esto fue seguido por la identificación de las condiciones operativas más adecuadas para la recuperación de antimonio a partir de voltamperogramas obtenidos mediante voltamperometría de barrido lineal.

En la fase final, se llevaron a cabo experimentos de electrodeposición galvanostática y potenciostática utilizando las densidades de corriente y potenciales previamente determinados. La efectividad de la recuperación de antimonio se evaluó mediante espectroscopía de absorción atómica.

Palabras Clave: Antimonio, Disolvente verde, Disolvente eutéctico profundo, Oxalina, Voltamperometría cíclica, Electrodeposición, Material prima crítico, Recuperación de antimonio.

RESUM

La Comissió Europea emet una llista anual de substàncies que es declaren com a Matèries Primeres Crítiques. Aquesta llista inclou metalloide, com l'antimoni, que són de rellevància especial per a la indústria i estan en risc de subministrament.

L'antimoni, encara que està present com a impuresa en els efluents generats per la indústria del coure, té una àmplia aplicació en diversos camps. Serveix com a component crucial en bateries de metall líquid i en la fabricació de semiconductors, com detectors infrarojos i díodes. A més, s'utilitza àmpliament com a catalitzador en la producció de tereftalat de polietilè (PET) i com a retardant de flama en cables, tèxtils i plàstics.

La recuperació d'antimoni present en residus sòlids generalment implica l'ús d'àcids inorgànics altament concentrats per a dissoldre el metall. La separació selectiva de l'antimoni del lixiviat o efluent resultant es pot dur a terme mitjançant electrodeposició.

Aquest estudi es centra en la utilització d'una alternativa ecològica als solvents clàssics per a la dissolució i recuperació d'antimoni. El solvent verd utilitzat en aquesta investigació és el solvent eutèctic profund, oxalina, que es compon de quantitats equimolars de clorur de colina i àcid oxàlic.

En aquesta Tesi de Màster, s'ha estudiat la dissolució d'antimoni en oxalina i la seua posterior recuperació mitjançant electrodeposició. Primer, s'ha realitzat la caracterització electroquímica d'oxalina i oxalina amb antimoni dissolt mitjançant voltamperometria cíclica. A continuació, s'han identificat les condicions operatives més adequades per a la recuperació d'antimoni a partir de voltamperogrames obtinguts mitjançant voltamperometria d'escaneig lineal.

En la fase final, es van dur a terme experiments d'electrodeposició galvanostàtica i potenciostàtica utilitzant les densitats de corrent i potencials prèviament determinats. L'efectivitat de la recuperació d'antimoni es va avaluar mitjançant anàlisis per espectroscopia d'absorció atòmica.

Paraules clau: Antimoni, Dissolvent verd, Dissolvent eutèctic profund, Oxalina, Voltamperometria cíclica, Electrodeposició, matèries primeres crítiques, Recuperació d'antimoni.

TABLE OF CONTENT

LIST OF FIGURES

LIST OF TABLES

LIST OF ACRONYMS AND ABBREVIATIONS

AAS	Atomic Absorption Spectroscopy
CE	Counter Electrode
CRM	Critical Raw Material
CV	Cyclic Voltammetry
DES	Deep Eutectic Solvent
DSA	Dimensionally Stable Anode
E	Potential
EoL	End-of-Life
HBA	Hydrogen Bond Acceptor
HBD	Hydrogen Bond Donor
HCl	Hydrochloric Acid
HER	Hydrogen Evolution Reaction
i	Current Density
i_L	Limiting Current Density
ILs	Ionic Liquids
LSV	Linear Sweep Voltammetry
MMO	Mixed Metal Oxide
OCP	Open Circuit Potential
PET	Polyethylene Terephthalate
ppm	Parts Per Million
RDE	Rotating Disk Electrode

RE	Reference Electrode
Sb	Antimony
SCE	Saturated Calomel Electrode
SCF	Supercritical Fluids
SDG	Sustainable Development Goal
SHE	Standard Hydrogen Electrode
WE	Working Electrode

Part I

Memoir

Chapter 1

Introduction

1.1. Antimony: An Overview

Antimony, symbolized as Sb, is a semi-metallic element with the atomic number 51. Though it is not a common element in Earth's crust, with an estimated abundance ranging from 0.2 to 0.5 parts per million [1], it can be found in over 100 mineral species. Table 1 presents some of the more common antimony containing minerals that are found in nature.

Table 1: Some of the more common antimony minerals found in nature.

Common antimony minerals			
Andorite	$PbAgSb_3S_6$	Horsfordite	Cu_5Sb
Aurostibite	$AuSb_2$	Jamesonite	$Pb_4FeSb_6S_{14}$
Berthierite	$FeSb_2S_4$	Kermesite	Sb_2S_2O
Boulangerite	$Pb_5Sb_4S_{11}$	Livingstonite	$HgSb_4S_8$
Bournonite	$PbCuSbS_3$	Meneghinite	$CuPb_{13}Sb_7S_{24}$
Breithauptite	NiSb	Senarmontite	Sb_2O_3
Cervantite	Sb_2O_4	Stenhuggarite	$CaFeSbAs_2O_7$
Cylindrite	$Pb_3Sn_4FeSb_2S_1$	Stephanite	Ag_5SbS_4
Dyscrasite	Ag_3Sb	Stibiconite	$Sb_3O_6(OH)$
Falkmanite	$Pb_3Sb_2S_6$	**Stibnite**	**Sb_2S_3**
Famatinite	Cu_3SbS_4	Tetrahedrite	$(Cu,Fe)_{12}Sb_4S_{13}$
Franckeite	$Pb_5Sn_3Sb_2S_{14}$	Ullmannite	NiSbS
Freibergite	$(Ag,Cu,Fe)_{12}(Sb,As)_4S_{13}$	Valentinite	Sb_2O_3
Gabrielite	$Tl_6Ag_3Cu_6(As,Sb)_9S_{21}$	Tetrahedrite	$(Cu,Fe)_{12}Sb_4S_{13}$
Geocronite	$Pb_{14}(Sb, As)_6S_{23}$	Zinkenite	$Pb_9Sb_{22}S_{42}$

Antimony is primarily found in nature as the gray sulfide mineral stibnite (Sb_2S_3), also known as *'Stibium'* in Latin, which is the origin of its standard chemical symbol 'Sb'.

According to the World Mining Data (WMD) [2], there was a downward trend in the global mine production of antimony from 2018 to 2022. The production decreased from 145,002

tons in 2018 to 83,031 tons in 2022, marking a decrease of -42.74%. The significant decrease in production primarily stems from China, which produced up to 70,396 tons of raw materials in 2018. However, this figure decreased over the years to 39,000 tons in 2022.

Despite the substantial decrease, China remains the leading producer. Its production of 39,000 tons accounts for 47.68% of the world's total production. Tajikistan follows China in second place, producing 14,500 tons, which constitutes 17.46% of the global total. Türkiye ranks third, contributing 12.81% to the world's total antimony production with a yield of 10,640 tons.

1.1.1. Applications

Antimony, a versatile element, is used in a wide range of applications. Figure 1 illustrates its primary applications based on the percentage distribution provided in the SCRREEN report, 'Solutions for Critical Raw Materials - a European Expert Network' [13].

Here are some of antimony's key uses:

- **Flame Retardants:** Antimony trioxide is a key ingredient in flame retardants, accounting for about 43% of global antimony usage. It is incorporated in a variety of materials such as plastics, cable coatings, furniture, car seats, fabrics, and household appliances to enhance their fire resistance.

- **Battery Manufacturing:** Hard-lead alloys, also known as antimonial alloys, are integral to the production of lead-acid batteries. This application represents approximately 32% of the world's antimony consumption.

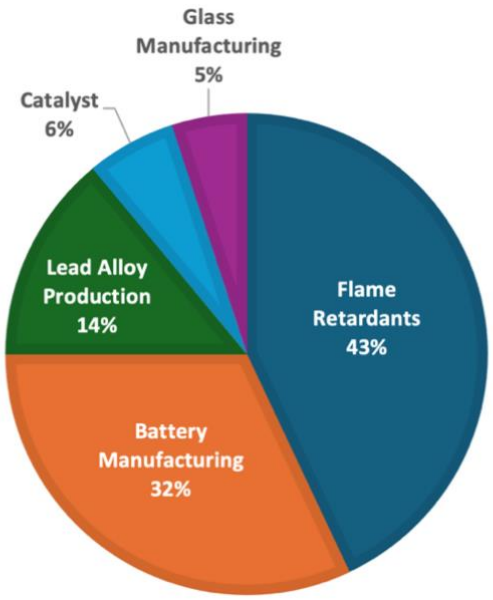

Figure 1: Antimony applications chart.

- **Lead Alloy Production:** Lead alloys, which are made harder by the addition of antimony, are used in the manufacture of low-load bearings in the automotive sector and in the creation of household and decorative items. This sector accounts for about 14% of global antimony use.

- **Catalyst**: Antimony trioxide serves as a catalyst in the production of polyethylene terephthalate (PET), accounting for around 6% of antimony usage.

- **Glass Manufacturing:** Sodium hexahydroxyantimonate, a form of antimony, is used in the production of high-quality clear glass. This application constitutes about 5% of the global antimony consumption.

1.1.2. Production of Antimony from stibnite ore

Antimony is primarily produced from the mineral stibnite (Sb_2S_3), which, as mentioned before, is the most significant natural source of the element. The main methods for producing antimony from stibnite are the Two-Step process and the Direct Reduction of stibnite, both of which are pyrometallurgical processes, as well as alkaline and acidic leaching, which are hydrometallurgical methods [14].

1.1.2.1. Two-step process

The main method for producing antimony is the pyrometallurgical two-step process. In this method, stibnite concentrate (Sb_2S_3) is roasted in an oxidizing environment, converting it into antimony trioxide (Sb_2O_3) [15, 16]. This reaction takes place at temperatures between 350-500°C and is represented by Equation 1:

$$2Sb_2S_3 + 9O_2 \rightarrow 2Sb_2O_3 + 6SO_2 \quad (1)$$

In the second step, the antimony trioxide is reduced in a blast furnace with carbon (typically coke) as the reducing agent [17]. This reduction process occurs at temperatures around 1000-1300 °C and produces metallic antimony and carbon monoxide, as shown in Equation 2.

$$Sb_2O_3 + 3\mathrm{C} \rightarrow 2\mathrm{Sb} + 3\mathrm{CO} \quad (2)$$

1.1.2.2. Carbothermic Reduction

The second method involves the direct reduction of stibnite. In this process, stibnite is mixed with a reducing agent, such as hydrogen, carbon, or carbon monoxide, and a sulfur capture agent, like CaO or $CaCO_3$. The mixture is then heated to high temperatures in a blast furnace,

resulting in the formation of metallic antimony, calcium sulfide, and carbon dioxide [17]. Equation 3 represents the chemical reaction for the carbothermic reduction of stibnite ore.

$$2Sb_2S_3 + 6CaO + 3C \rightarrow 4\mathrm{Sb} + 6\mathrm{Ca}S + 3CO_2 \quad (3)$$

This method simplifies the production process by eliminating the intermediate step of producing antimony trioxide.

1.1.2.3. Hydrometallurgical route

The third method is the hydrometallurgical route. In this process, stibnite ore is subjected to an alkaline or acidic leaching, converting the stibnite concentrate into a soluble antimony solution. The leach solution is then purified to remove impurities, and antimony is precipitated out of the solution, often as antimony trioxide or antimony metal.

The antimony obtained from all these methods can be further refined through processes such as liquation, electrolysis, or zone refining to achieve the desired purity. While all three methods are effective, the two-step roasting and reduction process is most widely used because it allows for the effective removal of sulfur and other impurities, resulting in a higher quality final product. Additionally, the roasting step can be controlled to produce antimony trioxide directly, which, as discussed previously, is one of the main forms of antimony used in various applications. Furthermore, the hydrometallurgical route is gaining attention for its environmental benefits and suitability for complex ores.

1.2. Sustainable Recovery of Antimony from Effluents

1.2.1. The Importance of Antimony Recovery

As previously mentioned, antimony plays a significant role as an industrial raw material. The European Commission has classified antimony as a Critical Raw Material (CRM). CRMs are defined as raw materials for which there are no viable substitutes with the same performance characteristics, and which are of high economic importance to the European Union (EU) [3].

Mining and production of antimony ores or concentrates is not carried out within the EU. As a result, the EU is entirely dependent on imports, establishing it as a net importer with a complete, 100% reliance on external sources primarily on China. This dependency underscores the importance of antimony to the EU's economy. The EU’s economy, along with its key industries, is heavily reliant on these materials, which are at a significant risk of supply disruption. The recovery of antimony is therefore not only an environmental consideration, but also an economic one.

By recovering antimony from effluents, the dependence on primary sources of antimony, which are often associated with significant environmental and socio-economic impacts, can be reduced. Furthermore, in metallurgical industries such as those involved in the production of copper, gold, or lead, antimony, along with other elements like bismuth (Bi) and arsenic (As), are seen as impurities. The presence of these impurities can negatively affect the final product's quality, thereby necessitating their removal.

Moreover, the recovery process can potentially be more energy efficient than the extraction and refining of primary antimony, which aligns with the United Nations' Sustainable Development Goals (SDGs), as shown in Chapter 2.

1.2.2. Antimony Recovery Process

The continuing growth in the supply-demand gap for antimony, as mentioned in the CRMs report by the European Commission, resulted in efforts to find secondary sources of antimony [3, 14]. These efforts primarily focus on two secondary sources:

- **Recycling of End-of-Life Products (EoL):** Antimony is often recovered from spent lead-acid batteries, where it is directly reclaimed as a lead-antimony alloy. Additionally, end-of-life solar panel glass containing antimony is another potential source that is being considered for mandatory recycling [14].
- **Recovering Antimony from Industrial Process Effluents:** Valuable residues presenting high antimony content can be, as mentioned before, obtained from metallurgical industries such as from the processing of gold, copper, and lead ores. These residues, which are often discarded or stockpiled, pose environmental concerns and represent a significant opportunity for antimony recovery.

In the context of copper, which is also a crucial industrial metal, it is primarily extracted from ores such as Chalcopyrite ($CuFeS_2$), Bornite (Cu_5FeS_4), Malachite ($Cu_2CO_3(OH)_2$), and copper sulfides including Enargite (Cu_3AsS_4) and Chalcocite (Cu_2S). These ores, however, often contain impurities, such as antimony, arsenic, and bismuth. The presence of these impurities requires complex purification processes during copper production, resulting in high purity copper cathodes (99.9%). The block diagram shown in Figure 2 gives the typical steps of the multi-stage pyrometallurgical copper production process starting from copper sulfide ores:

1. **Mining**: This is the first step where the copper ore is physically removed from the ground. This can be done through open-pit (surface) mining or underground mining depending on the location and quality of the ore.

2. **Comminution (Crushing and Milling)**: The extracted copper ore is then crushed and ground into a fine powder. This increases the surface area of the ore particles, which helps in the subsequent concentration step.

3. **Concentration**: Once the ore has been milled, it is subjected to a process called froth flotation. In froth flotation, the ground ore is mixed with water to form a slurry. Chemical reagents are added to the slurry to bind to the copper minerals, making them hydrophobic (water-repelling). The slurry is then agitated, creating bubbles. The hydrophobic copper minerals attach to the bubbles and float to the top of the slurry, while the waste rock sinks. The copper-rich froth at the top is then skimmed off, leaving the waste rock at the bottom. The froth is then dried to form a copper-rich powder, which is forward to the next processing stage.

4. **Smelting**: The smelting stage involves the oxidation of copper-rich powder from the 'Concentration' step to produce a molten 'Copper matte' and a slag. The smelting process takes place in a furnace at an approximate temperature of 1200 °C. Oxygen-enriched air is blown into the furnace, along with dried concentrate, a flux agent (SiO_2), and recycled materials from different stages of the process.

   This slag, encapsulating the waste material from the ore, is segregated and removed [4].

5. **Conversion**: In this stage, iron and sulfur from copper ores are removed, resulting in a product that is nearly 99 % copper, which is called 'Blister copper' named after its appearance. The process involves blowing oxygen-enriched air at low pressure into the molten copper matte. The conversion process occurs in two sequential stages:

   - In the first stage, iron is selectively oxidized over sulfur to form iron oxide (FeO), which then reacts with the added silica flux to form an iron silicate (fayalite)-based slag, as shown by Equation 4.

   $$2FeO + SiO_2 \rightarrow Fe_2SiO_4 \quad (4)$$

   - In the second stage, given by Equation 5, the sulfur attached to the copper is oxidized, forming SO_2 gas until elemental copper with a concentration of approximately 99 % purity is obtained.

   $$2CuS + 3O_2 \rightarrow 2Cu + 2SO_2 \quad (5)$$

   This SO_2-gas is extracted and utilized in the production of sulfuric acid, leaving behind the elemental 'Blister' copper.

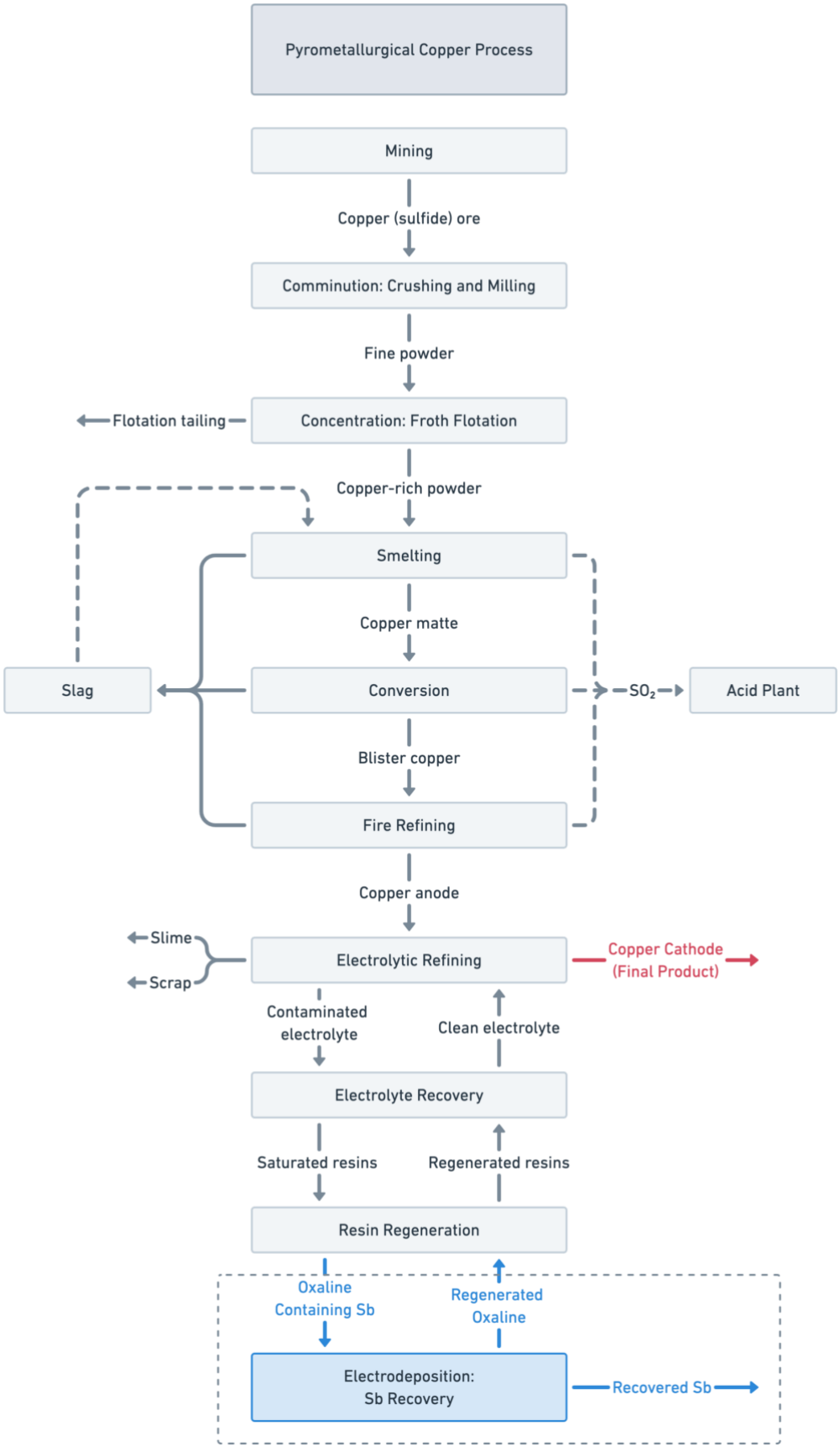

Figure 2: Block diagram of pyrometallurgical copper process.

6. **Fire Refining**: This process is designed to further purify the 'blister' copper and prepare it for the final electrolytic refining step.

   The fire refining process is divided into two main stages: oxidation and reduction. During the oxidation stage, air is introduced into the molten 'blister' copper. The oxygen in the air reacts with the sulfur and other impurities in the copper, forming a refining slag. This slag, which contains the oxidized impurities, is then separated from the copper.

   After the oxidation stage, the material is forwarded to the reduction stage, where a reducing agent, typically butane gas, is blown into the furnace. The purpose of this step is to remove the remaining oxygen in the copper. The result of this stage is copper that has been refined to a purity of approximately 99.7 % and is used as an anode in the next electrorefining step.

7. **Electrolytic Refining:** Also known as electrorefining, is another key process in pyrometallurgical copper production. This process involves the electrolytic dissolution of the 99.7 % (impure) copper anodes, and the selective electroplating of the dissolved copper to form a pure (99.99 %) copper cathode.

   The process takes place in a cell containing an electrolyte, which is mainly a copper sulfate and sulfuric acid solution. When an electric current is applied, copper ions from the anode dissolve into the electrolyte (they are oxidized). These copper ions are then reduced at the cathode, depositing pure copper. The electrorefining step offers good selectivity, so that the impurities remain in the anode slimes and can further be processed.

8. **Electrolyte Recovery:** During electrolysis, most impurities remain in the electrolyte solution, while others form a precipitate at the bottom of the cell, which can be easily separated by mechanical methods. In this stage, the contaminated electrolyte undergoes an ion-exchange process, where it is passed through aminophosphonic resins. These resins have a high affinity for certain metals, primarily antimony (Sb) and bismuth (Bi), which are adsorbed by the resin. This process purifies the electrolyte effectively, allowing for its reuse in the copper electrorefining process.

9. **Resin Regeneration:** After several cycles of electrolyte recovery of the electrorefining baths, the ion-exchange resins become saturated with impurities. These resins then undergo a regeneration process to restore their ion-exchange capacity. This process typically involves passing an eluate solution through the resin, effectively 'cleaning' it by displacing the bound metals.

   - **Previous Work:** In previous work, the resin regeneration was conducted using a concentrated solution of hydrochloric acid (5-7 M). The addition of HCl serves

a dual purpose: it increases the solubility of antimony in the solution and prevents the hydrolysis of antimony.

However, the use of HCl presents a set of challenges. It is a corrosive substance that poses significant environmental, safety, and equipment concerns. As a strong acid, HCl contributes to environmental acidification, affecting water streams, soil health, and more. From a safety perspective, it poses a serious inhalation hazard, and contact with it can result in severe skin burns and eye damage. Additionally, the corrosive nature of HCl can lead to significant equipment damage, particularly to metals.

- **Current Research:** Due to the negative properties of HCl, the focus of the present study is to replace this inorganic solvent used in the elution of the ion exchange resin of the copper production process by safer and more environmentally friendly solvents. Green solvents, like deep eutectic solvents, specifically the eutectic solvent “Oxaline”, is considered as an alternative to traditional solvents, such as HCl, in the recovery of metals like Sb.

10. Subsequently, the recovery of antimony from the resulting eutectic solvent, or previously HCl, can be conducted by means of electrodeposition, which is included at the bottom of the block diagram shown in Figure 2.

1.3. Green Solvents

In the context of green chemistry, green solvents have become a focal point, particularly following the United Nations’ sustainability-oriented development plan of 2015. This plan highlighted the central function of green chemistry and, by extension, green solvents in the pursuit of a sustainable future. Green solvents, primarily sourced from renewable resources such as agricultural products or other sustainable practices, are proposed as substitutes for traditional (petrochemical) solvents. Their key features include recyclability, biodegradability, and reduced toxicity.

The formulation and application of green solvents are guided by the 12 principles of green chemistry, which advocate for the reduction or eradication of hazardous substances [21, 22]. As a result, green solvents are designed to minimize waste, lower toxicity, and improve energy efficiency, thereby lessening the environmental footprint of chemical processes.

There are several types of green solvents, including Supercritical fluids, deep eutectic solvents, and Ionic Liquids.

Supercritical fluids (SCFs) are a unique state of matter that occurs when a substance surpasses its critical temperature and pressure, resulting in the disappearance of distinct liquid and gas

phases [23]. This supercritical state exhibits properties that differ significantly from those of gases or liquids under standard conditions. This supercritical state combines the properties of gases and liquids, allowing SCFs to penetrate materials like a gas and dissolve substances like a liquid. These fluids possess high density and low viscosity, which are advantageous for various applications. Among SCFs, supercritical carbon dioxide ($scCO_2$) is the most widely used due to its moderate critical temperature (31.3 °C) and pressure (73.8 bar). $scCO_2$ is non-toxic, non-flammable, chemically inert, and relatively inexpensive, making it an ideal solvent for many applications [23].

Ionic Liquids (ILs) are essentially salts in a liquid state composed of ions, which remain liquid at temperatures below 100 °C, and often even at room temperature, hence they are also referred to as room-temperature ionic liquids (RTILs). ILs are non-volatile, meaning they do not evaporate easily, making them ideal for tasks where controlling emissions is crucial. They also possess high thermal stability, excellent solvation potential for a wide range of substances, and the ability to dissolve various organic and inorganic materials [24].

However, while SCF, ILs, and Deep Eutectic Solvents (to be discussed in the following paragraph) are labeled as ‘green solvents’, the environmental implications of these solvents depend on their specific chemical composition and the processes in which they are used.

1.3.1. Deep Eutectic Solvents

As mentioned in the previous chapter, Deep Eutectic Solvents (DES) are another type of green solvent. They are a relatively new concept in the field of green chemistry, but despite their recent introduction, they have already been the subject of numerous publications spanning various research areas and fields of application [8].

The term “eutectic” is derived from the Ancient Greek word εὔτηκτος or eútēktos, which translates to “easily melted”. As can be seen in Figure 3, the term eutectic (point) is used to describe the chemical composition and temperature at which a mixture of two solids becomes fully molten at the lowest melting temperature relative to either compound.

The lower melting point of a DES compared to its individual constituents is attributed to three key factors: intermolecular interactions, lattice structure, and entropy.

When a DES is formed, the substances interact to create new intermolecular bonds. These new bonds are typically weaker than the original bonds in the individual substances. This is due to the fact that the formation of a DES often involves the creation of relatively weak hydrogen bonds, as opposed to the stronger ionic, covalent, and/or hydrogen bonds present in the pure substances. Furthermore, the creation of these new bonds disrupts the structured lattice of the individual substances. This disruption facilitates the transition of the substance from a solid to a liquid state, effectively reducing the melting point. In addition, the formation

of these new bonds increases the system's disorder, or entropy. An increase in entropy is thermodynamically favorable, meaning the system will naturally gravitate towards states with higher entropy. Given that a liquid state is more disordered than a solid state, the formation of a DES promotes the transition to a liquid state, further reducing the melting point.

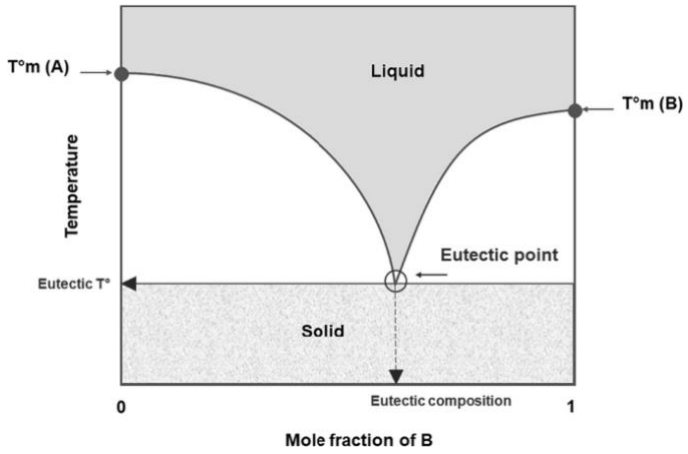

Figure 3: Phase diagram of a binary system that forms an eutectic mixture. Source: adapted from [5].

DES are typically defined as binary or ternary mixtures that are capable of self-association, often through hydrogen bond interactions, to form an eutectic mixture. The eutectic mixture has a melting point ($T_{eutectic}$) that is lower than that of each individual component, T°m(A) and T°m(B). As a result, these solvents typically remain in a liquid state at temperatures below 100 °C.

Eutectic solvents are formed from two or more components. The general formula for a DES involves a cation (Cat^+), a Lewis base (X^-), a Lewis or Brønsted acid (Y), and a variable (z) representing the number of Y molecules [6], and can be described as formula 6:

$$Cat^+X^- \cdot zY \tag{6}$$

The cation (Cat^+) can be an ammonium, phosphonium, or sulfonium, but it is generally a quaternary ammonium. The Lewis base (X^-) is usually a halide anion like chloride. The most researched and widely used Cat^+X^- combination is the quaternary ammonium salt, choline chloride, which is also the one that is used in this research.

Eutectic solvents can be classified into four distinct types [8], as illustrated in Figure 4. The classified is mainly based on the Lewis or Brønsted acid (Y) used in the general formula. Each type represents a unique combination of components, which offer a distinct set of properties and potential applications. Type I is formed when a metal chloride is used. Type II is characterized by the use of a hydrated metal chloride [6].

Type III DES represent a distinct category within the broader class of metal-free solvents. The formation of these solvents involves the combination of a Hydrogen Bond Donor (HBD) and a Hydrogen Bond Acceptor (HBA).

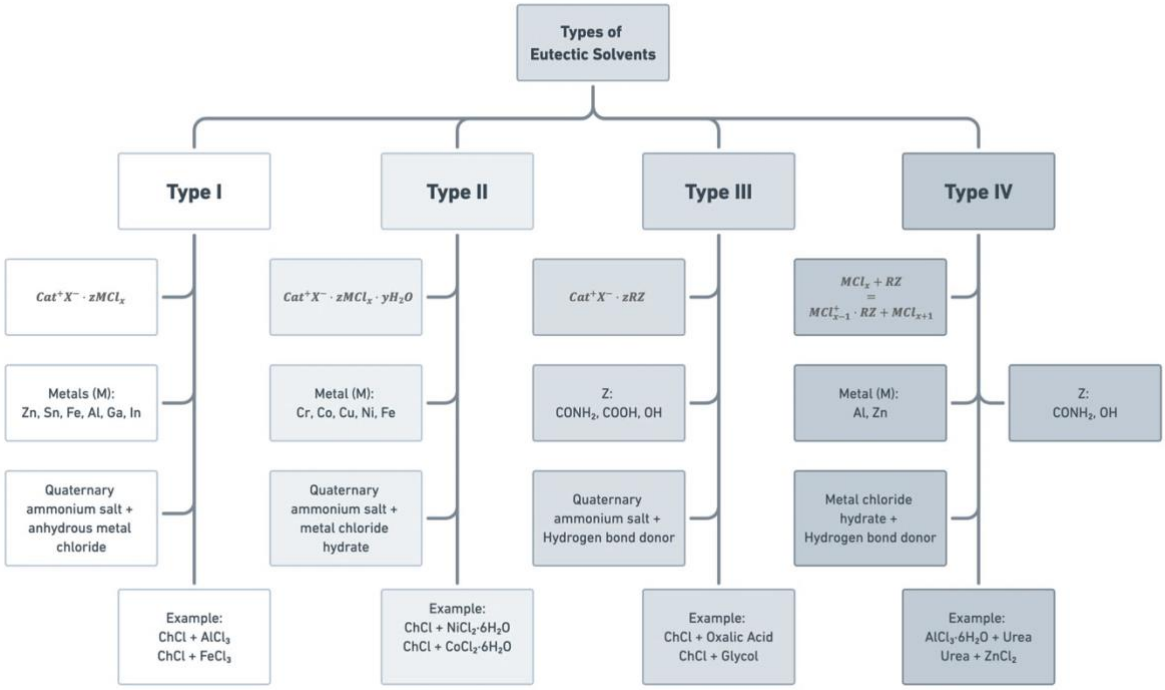

Figure 4: Classification of DES.

Extensive research on numerous HBD has resulted in the type III DES most commonly made from amides, carboxylic acids, and alcohols [7, 8]. Figure 5 illustrates a selection of frequently used HBA and HBD, with choline chloride as the most preferred HBA.

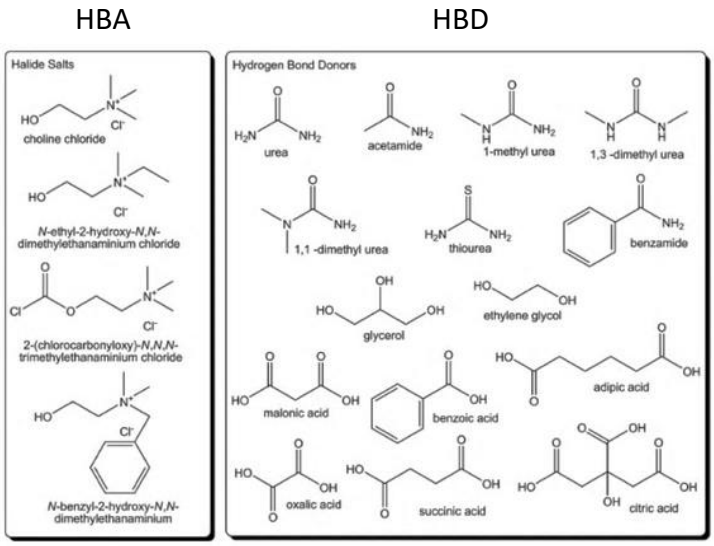

Figure 5: Frequently used HBA and HBD in the preparation of DES [8].

The adaptability of a Type III DES is particularly notable due to the wide range of available HBD. This diversity allows for a high degree of flexibility in the design and application of these

solvents, meaning that the characteristics of the DES can be adjusted to meet the requirements of various industrial processes.

This type of DES exhibits a great ability to solvate a diverse array of transition metal species, including chlorides and oxides [8]. This wide-ranging solvation capability has led to the use of a Type III DES in this research. Some common type III DES combinations, with choline chloride as the HBA, include:

- **Choline chloride and Urea:** This is one of the most studied combinations and is known as 'Reline'.
- **Choline chloride and Ethylene glycol:** Another well-known DES, with ethylene glycol serving as the HBD. This combination is called 'Ethaline'.
- **Choline chloride and Malonic acid:** This combination utilizes malonic acid as the HBD and is referred to as 'Maline'.
- **Choline chloride and Oxalic acid:** The eutectic solvent, named 'Oxaline,' is used in this research and is discussed further in Chapter 3, Section 3.1.1: ‘Preparation of the Deep Eutectic Solvent: Oxaline’.

Lastly, Type IV DES are formed when an organic HBD compound reacts with a metal chloride [8]. For example, zinc chloride ($ZnCl_2$) and ethylene glycol, or iron(III)chloride ($FeCl_3$) and urea.

1.4. Electrolytic Cell

An electrolytic cell is a type of cell that drives a non-spontaneous redox reaction through the application of electrical energy. This is in contrast to a galvanic cell, which generates electrical energy from a spontaneous redox reaction.

1.4.1. Basic Principle

The operation of an electrolytic cell revolves around the concept of electrolysis. This is a process where electrical energy is used to drive a non-spontaneous chemical reaction.

The operation of an electrolytic cell involves the flow of ions through the electrolyte and the flow of electrons through the external circuit. When the power source is connected, it creates a potential difference between the anode and the cathode. This causes the ions in the electrolyte to migrate towards the electrodes.

Cations (positively charged ions) move towards the cathode where they undergo reduction, while anions (negatively charged ions) move towards the anode where they undergo

oxidation. The electrons produced at the anode travel through the external circuit to the cathode, completing the electrical circuit.

1.4.2. Simple Electrolytic Cell Setup

The provided diagram (Figure 6) represents a basic electrolytic cell and its key components: two electrodes (the anode and the cathode), the electrolyte, and the power source with connections to the electrodes. The power source provides the energy necessary for the non spontaneous reaction.

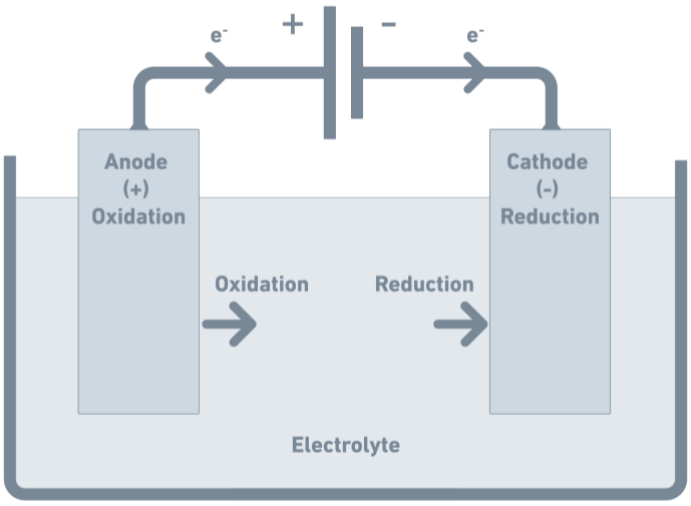

Figure 6: Diagram of a simple Electrolytic Cell.

The anode connected to the positive (+) terminal of the power source, is the electrode where oxidation takes place. Oxidation is the process characterized by a substance losing electrons. The general reaction at the anode (Oxidation) can be represented as Equation 7:

$$Red \rightarrow Ox + n\, e^{-} \tag{7}$$

This represents the loss of electrons by the reducing agent (Red), which gets converted into an oxidized form (Ox).

On the other hand, the cathode, generally connected to the negative (-) terminal of the power source, is the electrode where reduction takes place. This is a process characterized by a substance gaining electrons. The general reaction at the cathode (Reduction) can be represented as Equation 8:

$$Ox + n\, e^{-} \rightarrow Red \tag{8}$$

This represents the gain of electrons by the oxidizing agent (Ox), which gets converted into its reduced form (Red).

In these equations, n represents the number of electrons transferred during the reaction. The specific species and the number of electrons depend on the electrolyte and the particular redox reactions taking place in the electrolytic cell.

As previously mentioned, when the circuit is closed and the electric supply is turned on, reactions occur at the electrodes. Electrons released at the anode (oxidation) flow towards the cathode (reduction), forming an electric current through the external circuit. The direction of this electron flow is indicated by arrows in the accompanying diagram (Figure 6).

1.4.3. Electrodes

As previously explained and shown in Figure 6, a two-electrode setup can be used for an electrolytic cell. However, in most cases, a three-electrode setup is preferred for more precise control and measurement of the electrochemical reactions. This setup includes a working electrode, a counter electrode, and a reference electrode [25].

Working Electrode (WE): The WE is where the reaction of interest occurs. This electrode is monitored for changes in current or potential. The material of the working electrode can vary depending on the specific experiment or application.

Counter Electrode (CE): The CE, also known as the auxiliary electrode, is used to balance the charge in the system. The reactions that occur at the counter electrode are not typically of interest in the experiment. Its main purpose is to provide a path for the current to complete the circuit.

Reference Electrode (RE): The RE has a stable and well-known electrode potential. The potential of the WE is usually controlled and measured with respect to the reference electrode. Common examples of reference electrodes include the Standard Hydrogen Electrode (SHE), the Saturated Calomel Electrode (SCE), and the Silver/Silver Chloride Electrode (Ag/AgCl).

In a three-electrode setup, the working and counter electrodes are connected to the power source, while the reference electrode is connected to the voltmeter along with the working electrode. This setup allows for more accurate control and measurement of the potential at the working electrode, which is crucial in many electrochemical experiments and applications.

The reactions at the working electrode are driven by the potential difference between the working electrode and the reference electrode. This setup allows for precise control over the electrochemical reactions occurring in the electrolytic cell.

Both two-electrode and three-electrode setups involve immersing the electrodes in an electrolyte. The electrolyte, which contains free ions, can be a liquid, gel, or solid. It conducts

electricity by the movement of ions and facilitates the flow of ions between the anode and cathode, which is essential for redox reactions to occur.

1.5. Cyclic Voltammetry

Cyclic voltammetry (CV) is an electroanalytical technique that measures the current response of a solution to a varying applied electrode potential. It is used to study the system before performing electrodeposition and other experiments like linear sweep voltammetry because it provides crucial information on the redox behavior of analytes, reaction kinetics, and mechanisms. This preliminary data helps in understanding the system's behavior, prior to the subsequent electrodeposition and linear sweep experiments [19].

1.5.1. Basic Principle

CV uses a three-electrode configuration, consisting of a working electrode, counter electrode, and reference electrode, as previously discussed. When a potential is applied between the working electrode and the reference electrode, oxidation or reduction reactions (depending on the applied potential) occur at the surface of the working electrode. This results in a flow of electrons to or from the counter electrode, generating a measurable current. The reference electrode maintains a constant potential, ensuring accurate measurement without significant current flowing through it [9].

Usually, the initial value of the applied potential at the start of a CV experiment is the Open Circuit Potential (OCP). This is the potential at which the system is in equilibrium, resulting in no net current flow. The OCP is specific to the system under study and can be influenced by factors such as the electrode material, the electrolyte, and the presence of any redox-active species. Starting the potential sweep from the OCP ensures that the initial state of the system is well-defined.

After establishing the equilibrium and thereby the OCP of the system, the potential is then swept to more positive or negative values, depending on the system and the sought-after information, until the first vertex potential is reached. The vertex potential is the minimum or maximum potential reached during the potential sweep. There are usually two vertex potentials in a cyclic voltammetry experiment: the forward vertex potential (also known as the switching potential) and the reverse vertex potential. The forward vertex potential is the potential at which the direction of the potential sweep first changes. The reverse vertex potential is the potential at which the direction of the potential sweep changes for the second time, returning to the initial potential, OCP.

The range between the vertex potentials defines the potential window of the experiment, which is crucial as it determines which redox reactions occur during the experiment. It should

be set to cover the redox potentials of the electroactive species in the system under study while avoiding potentials where solvent or electrolyte decomposition occurs, as this can interfere with the measurement or damage the electrode.

The rate at which the potential is changed (swept) over time during the experiment, is called the scan rate. It is typically measured in volts per second (V/s) or millivolts per second (mV/s). The scan rate can significantly influence the shape and size of the resulting voltammogram, and it provides valuable insights into the kinetics of the electrochemical reactions under study. In general, a high scan rate can lead to a larger current response and sharper peaks, useful for studying fast electron transfer reactions [9]. On the other hand, a low scan rate allows more time for the system to reach equilibrium, making it more suitable for studying slower processes.

Figure 7 illustrates the potential (in volts) over time (in seconds) for a typical cyclic voltammetry experiment. The initial potential applied between the working electrode and the reference electrode, in this illustrating example Figure 7, is -0.2 V (OCP). From this point, the potential decreases to the first (switching) vertex potential (E1), at which the potential is reversed. So, after reaching E1 the potential increases, passes the OCP until the second (reverse) vertex potential (E2) is reached. This happens with a scan rate, represented by the slope, in this case, 40 mV/s. After reaching E2, the potential is reversed again until it returns to the initial potential (OCP), completing the first cycle of the cyclic voltammetry experiment. Typically, multiple cycles are performed to activate the electrode surface and ensure reproducible results. In the example shown in Figure 7, the second cycle starts at the end of the first cycle, so at -0.2 V (OCP), and the potential window selected for this experiment ranges from -0.8 V to 1.2 V.

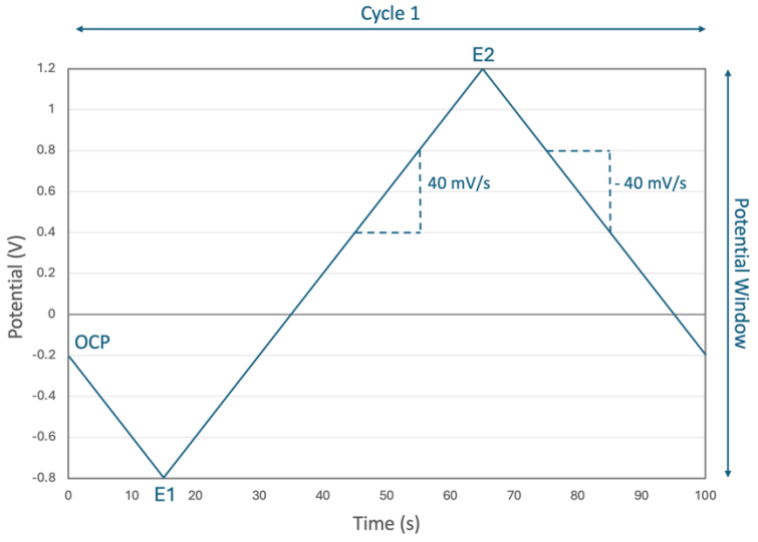

Figure 7: Example of the input signal applied during the registration of a cyclic voltammogram, showing potential sweep over time for a scan rate of (-)40 mV/s.

When the measured current density i (mA/cm^2) is plotted against the applied potential (V), a cyclic voltammogram is obtained, as shown in Figure 8. From these voltammograms, various electrochemical parameters can be obtained.

When the potential scans positively after reaching the switching potential, oxidation occurs. This results in the flow of an anodic current at the working electrode, which is a measure of the rate of oxidation at the surface of the electrode. The peak of this current, named the anodic peak current (i_{pa}) is reached when all the substrate present at the surface of the electrode is oxidized. The potential corresponding to this point is the anodic peak potential (E_{pa}) and represents the potential at which the oxidation reaction is most favorable [19, 20].

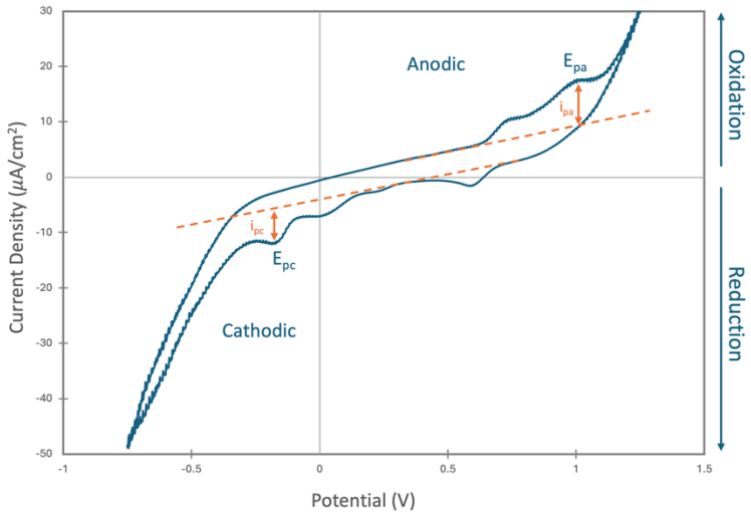

Figure 8: Example of the output response during the registration of a cyclic voltammogram, showing the measured current density over the applied potential.

On the other hand, the cathodic peak current (i_{pc}) and cathodic peak potential (E_{pc}) are related to the reduction process. When the potential is scanned negatively, reduction occurs and a cathodic current can be measured. This cathodic current is a measure of the rate of reduction at the surface of the electrode. The peak of this current, i_{pc}, is reached when all of the substrate at the surface of the electrode has been reduced. The potential at this point is the cathodic peak potential, E_{pc}. It signifies the potential at which the reduction reaction is most favorable.

The width and height of the peak for a particular process depends on the temperature, scan rate, rotation speed, type and concentration of the electrolyte, and the electrode material.

1.6. Linear Sweep Voltammetry

Linear Sweep Voltammetry (LSV) is another fundamental technique in the field of electrochemistry, and is most of the times done in addition to CV. But unlike CV, which

evaluates both half-reactions (oxidation or reduction), LSV focuses only on the analysis in one direction (Oxidation or reduction), the reaction of interest.

This type of voltammetry is used when the material of the working electrode is susceptible to damage at either anodic or cathodic potentials. The method involves monitoring the current at a working electrode while the potential between the working electrode and a reference electrode is linearly varied over time [26].

1.6.1. Basic Principle

LSV is similar to CV in that it is based on the three-electrode configuration. In LSV, however, a voltage sweep is applied in one direction, meaning that the applied voltage over the WE is either increased or decreased, but not reversed.

Consider Figure 9 as an illustrative example of the input signal applied during the registration of an LSV, showing the changing potential (in volts) over time (in seconds). In this example, the potential decreases from -0.02 V to -0.2 V over a period of 180 seconds. So, the rate at which the potential changes, known as the scan rate, is calculated as the slope of the potential vs. time curve. In this case, the scan rate is -10 mV/s, which is derived by dividing the total change in potential (-0.18 V) by the total time (180 seconds). The negative sign indicates that the potential is being swept in the negative direction.

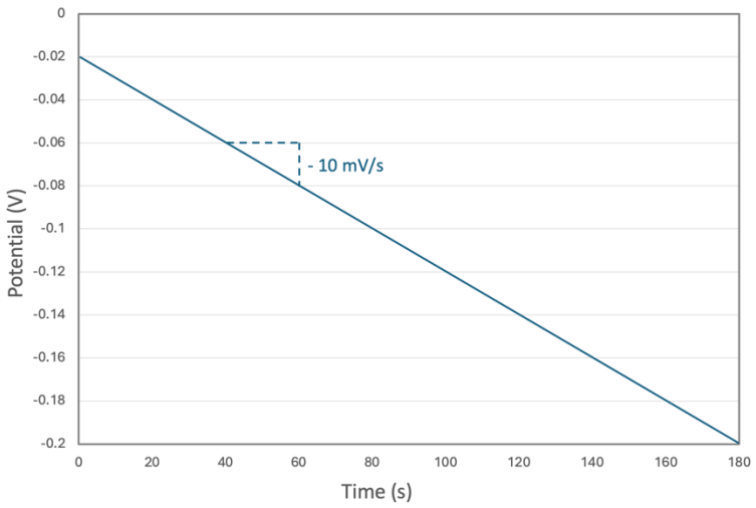

Figure 9: Example of the input signal applied during the registration of a linear sweep voltammogram, showing potential sweep over time for a scan rate of -10 mV/s.

As seen in the example (Figure 9), the potential applied to the working electrode during LSV experiments is swept linearly. The resulting current is measured, recorded, and displayed in a voltammogram, where the applied potential is plotted on the X-axis and the measured current density on the Y-axis, as shown in Figure 10. The characteristics of the linear voltammogram

depend on several factors, including temperature, rotation speed, electron transfer rate, chemical reactivity of the electroactive species, and scan rate.

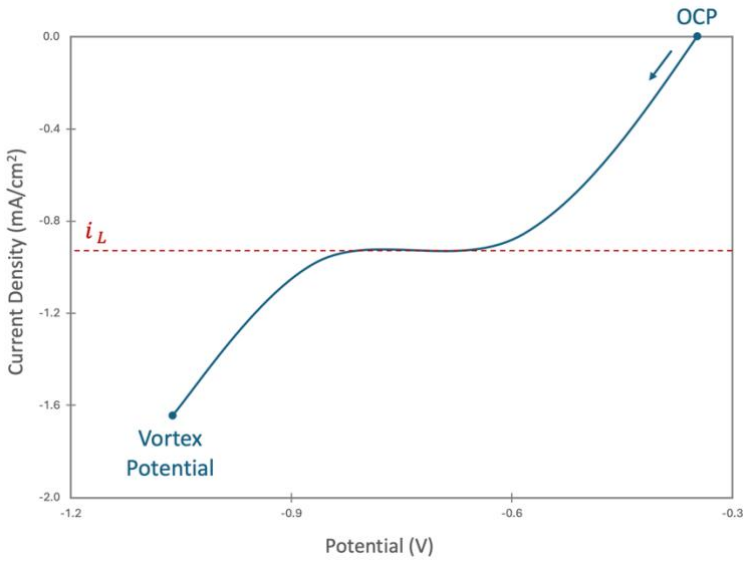

Figure 10: Example of a linear sweep voltammogram registered in the cathodic direction, showing the measured current density over the applied potential.

In the provided LSV graph (Figure 10), the potential is swept from the OCP in the cathodic direction towards more negative values. Initially, the current density increases, indicating the onset of a reduction process. The current continues to increase until it reaches a plateau, known as the limiting current density (i_L).

This plateau indicates that the maximum rate of mass transfer of reactants to the electrode has been reached. Beyond this point, increasing the electrode potential does not result in a significant increase of the current density. This is because the rate of the electrochemical reaction is now limited by how fast the reactants can diffuse to the electrode surface [18, 19].

However, if the potential is further increased beyond the plateau, the current density starts to rise again. This indicates that additional electrochemical processes are occurring. Possible explanations include the reduction of the medium, secondary reduction reactions involving different species, enhanced mass transport mechanisms, or changes in the electrode surface properties [19, 20].

In electrochemistry, the rate at which a reaction occurs can be limited by various factors, including the transfer of mass (usually ions or molecules) to the electrode surface. When the reaction rate is primarily limited by the rate at which reactants are transported to the electrode, rather than by the reaction kinetics at the electrode surface, it is said to be mass transfer controlled or diffusion limited [19].

1.7. Electrodeposition of Antimony

Electrodeposition is a process that uses an electric current to reduce dissolved metal cations, forming a thin, coherent metal layer on an electrode. This process is not only used to manufacture many products, including electronic components and devices, jewelry, and automotive parts, but also for the removal of certain metals from a solution. For instance, metals like Antimony can be removed from a solution through electrodeposition.

There are two main types of electrodeposition processes: potentiostatic and galvanostatic.

1.7.1. Potentiostatic Electrodeposition

During potentiostatic electrodeposition experiments, a constant potential is maintained across the electrodes, while the current density changes as a function of time. This change in current density, which is related to the rate of deposition, is monitored over time and usually depicted in a graph.

In potentiostatic electrodeposition, as well as in cyclic voltammetry and linear sweep voltammetry, the potential difference between the working electrode and the reference electrode is controlled by a potentiostat. A potentiostat functions by controlling the voltage difference between the working electrode and the reference electrode while measuring the current that flows between the working electrode and the counter electrode.

1.7.2. Galvanostatic Electrodeposition

Galvanostatic electrodeposition, also known as amperostatic electrodeposition, is a process where the current is kept constant during the deposition process, and the potential changes as a function of time. This method is often used in industrial applications where the rate of deposition is more important than the precise control of the deposit structure.

In galvanostatic electrodeposition, a constant current is passed through the cell, and the potential difference between the working electrode and the reference electrode is measured over time.

1.7.3. Potential and Current Density Determination

For both potentiostatic and galvanostatic experiments, the temperature and the rotation speed of the magnetic stirrer are held constant throughout the experiments. The potential values applied during the electrodeposition tests in potentiostatic mode and the current densities in the galvanostatic experiments were selected based on linear sweep voltammograms.

This selection process is illustrated in Figure 11, which is based on the example LSV curve registered in the cathodic direction, shown in Figure 10. Three specific points are selected:

- **Before the plateau (pre-peak):** At lower potentials and lower current densities (absolute values) than the peak.
- **At the plateau:** At the peak (or wave) reduction potential and the limiting current density (i_L) or peak current density.
- **After the plateau (post-peak):** At a higher absolute potential and corresponding higher current density (absolute values).

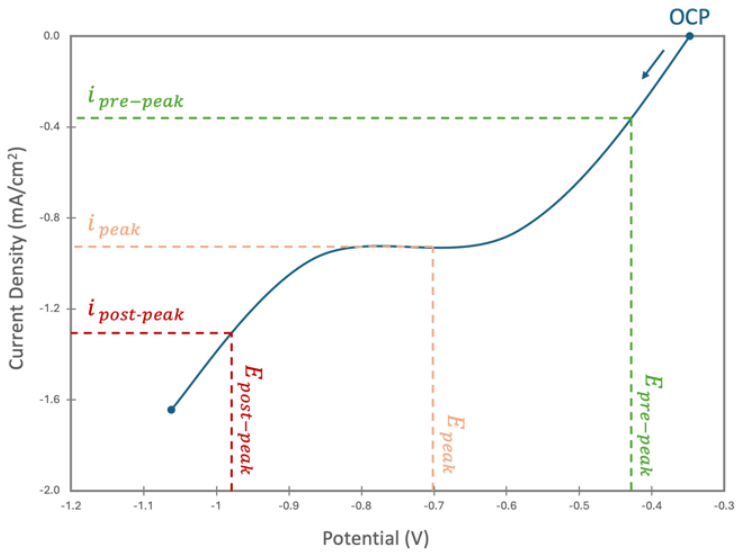

Figure 11: Example illustration of the selection of pre-peak, peak, and post-peak potentials and current densities for electrodeposition, based on the LSV curve in the cathodic direction.

1.8. Spectroscopic Analysis

Atomic Absorption Spectroscopy (AAS) is a widely used analytical technique for the detection of elements, like antimony in the samples from the electrodeposition experiments. The analysis technique of AAS is based on the principle that atoms of different elements absorb light (radiation) of specific wavelengths [28]. These wavelengths correspond to the energy difference between their ground and excited states. This unique characteristic of AAS allows for the quantification (and identification) of individual elements in a sample to a high accuracy.

1.8.1. Working Principle of AAS

The working principle of AAS involves several steps [27], which are given in the diagram of an Atomic Absorption Spectrometer (Figure 12).

The first step is “Sample Introduction and Nebulization”. In this step, a sample (such as those from the electrodeposition experiments) is introduced into the system through a capillary tube. The sample is then nebulized, which means that it is converted into a fine spray of droplets. This increases the surface area and facilitates its conversion into gaseous atoms in the next step.

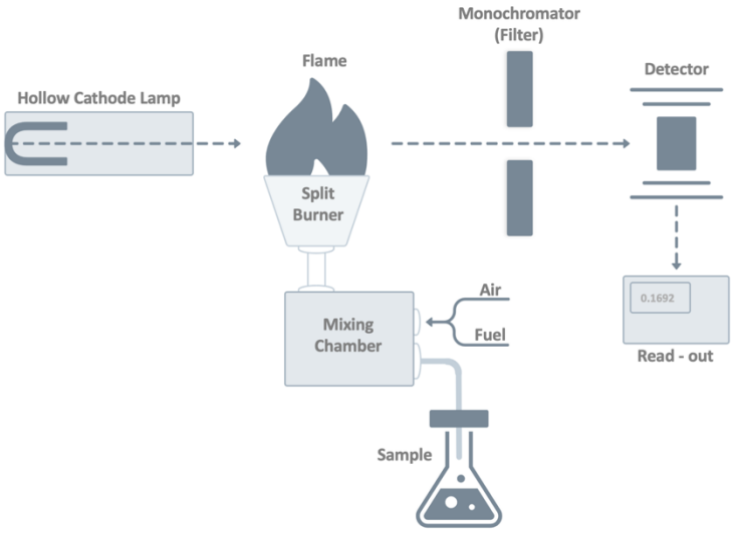

Figure 12: Simple Atomic Absorption Spectrometer configuration diagram.

The next step, “Atomization”, involves carrying the nebulized sample into a flame. The flame is formed from a continuous flow of ethylene (fuel) and air, which is directed to the nebulizer. The high temperature of the flame causes the sample to atomize, i.e., it is broken down into its constituent atoms. This is necessary because it is these atoms that absorb the light from the hollow cathode lamp in the “Radiation Absorption” step. Here, a hollow cathode lamp, which emits light of a specific wavelength corresponding to the element being analyzed, is directed at the flame. The atoms in the flame absorb this light and become excited.

The light that passes through the flame will reach the monochromator. The monochromator acts as a filter, allowing only light of the desired wavelength to pass through. This ensures that the detector only measures the light absorption of the specific element of interest. The light with this specific wavelength passes through the monochromator and is detected by the detector. The detector converts the light signal into an electrical signal, amplifies it, and records it. The recorded signal is proportional to the concentration of the element in the sample.

1.9. Previous Works on this topic

In previous research on this topic of the recovery of antimony from the elution solution during the ion-exchange resin regeneration step in the copper process, HCl was used. This previous work is depicted in the simplified block diagram shown in Figure 13.

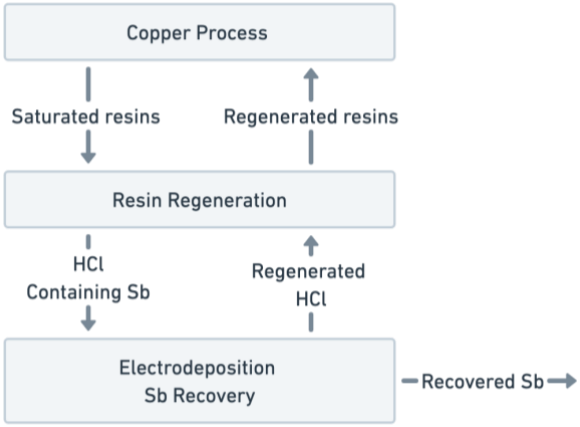

Figure 13: Simplified block diagram of the copper process and the area of research in previous work.

The 3-electrode configuration used in the LSV experiments of the previous work is similar to the setup used in this research. Both setups consist of a copper cathode (WE), a DSA anode (CE), and an Ag/AgCl reference electrode (RE). Additionally, a jacketed electrochemical cell is used in the current research instead of a beaker, allowing for precise temperature control. The used configuration for the current research is explained more in Chapter 3, Section 3.4.1: 'Experimental Setup'.

Figure 14 shows the LSV previously obtained for a 6 M HCl solution containing 2 mM antimony at three different rotation speeds (500, 700, and 950 rpm). The LSV indicates that the electrodeposition of Sb occurs at potentials more cathodic than -0.3 V vs. Ag/AgCl, and that the process is mass transfer-controlled, as denoted by the plateau at the limiting current density (i_L). At potentials higher than the limiting current density ($i > i_L$), the hydrogen evolution reaction (HER) predominates.

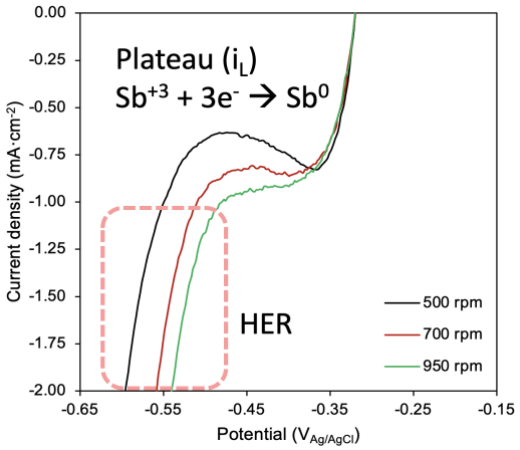

Figure 14: Previous work, Linear Sweep Voltammogram of a 6 M HCl solution containing 2 mM antimony at three different rotation speeds (500, 700 and 950 rpm), showing the HER at higher potentials as well as the limiting current density.

The potentiostatic electrodeposition of a 6 M HCl solution containing 2 mM antimony at a current density of 1.875 mA/cm² for 120 minutes results in a porous antimony deposit on the copper electrode. As shown previously by the LSV, at current densities higher than the limiting current density ($i > i_L$) the hydrogen evolution reaction (HER) predominates. This production of hydrogen gas leads to the porosity and detachment of the antimony deposit, as illustrated in Figure 15.

Figure 15: Previous work, potentiostatic electrodeposition at a current density of 1.875 mA·cm^{-2} for a duration of 120 min.

Chapter 2

Aim of this work

2.1. Master Thesis objective

The main objective of this thesis is to study the recovery of antimony from the elution solution used in the regeneration process of ion-exchange resins in copper electrorefining, as illustrated in Figure 16. This figure shows a simplified block diagram of the final steps in the pyrometallurgical copper process, previously discussed in Figure 2.

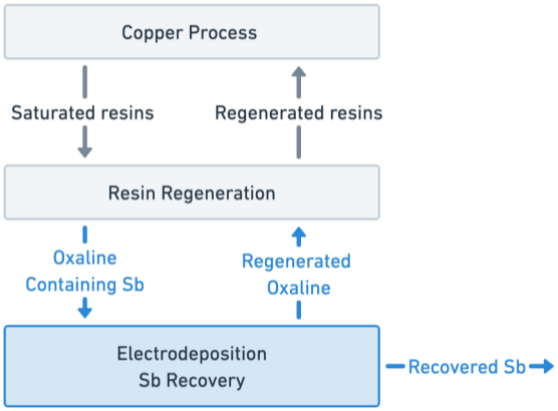

Figure 16: Simplified block diagram of the final steps in the pyrometallurgical copper process, highlighting the main objective of this master thesis. (Based on the full block diagram in Figure 2).

The solution used for regeneration, which removes antimony among other elements from the resin, a green solvent known as oxaline (deep eutectic solvent) is used. Subsequently, the antimony in the Oxaline is recovered using electrodeposition.

The main objective can be divided into several sub-parts.

1. **Oxaline preparation and antimony dissolution.**
    - Study the preparation of the eutectic solvent, oxaline.
    - Investigate the dissolution behavior of antimony in the prepared oxaline.

- Extra: Study the effects of HCl addition to the preparation and antimony dissolution steps.

Purpose: To establish a reliable and reproducible method for preparing oxaline with and without antimony.

2. **Electrochemical characterization using cyclic voltammetry.**

    - Characterization of the blank, oxaline without antimony.
    - Characterization of DES solutions with dissolved antimony under different conditions.

    Purpose: To gain information on the electrochemical reactions occurring within these systems from these cyclic voltammetric tests.

3. **Perform linear sweep voltammetry.**

    - Obtain the voltammograms of the oxaline solution with antimony under different conditions.
    - Extra: Study the effect of the addition of HCl on the linear sweep voltammograms.

    Purpose: To identify the most suitable operating conditions, including potentials and current densities, for the subsequent electrodeposition experiments. And thereby the optimal operating conditions determining for the recovery of antimony based on the obtained voltammograms.

4. **Electrodeposition experiments and deposition analysis.**

    - Perform galvanostatic electrodeposition experiments with the previously obtained current densities.
    - Perform potentiostatic electrodeposition experiments with the previously obtained potentials.
    - Evaluate the antimony electrodeposition using elemental analysis, specifically atomic absorption spectroscopy.

    Purpose: To study if the recovery of antimony from oxaline using electrodeposition under the studied conditions is feasible.

2.2. Sustainable Development Goals

The research conducted in this thesis intersects with several of the United Nations' Sustainable Development Goals (SDGs), demonstrating its relevance and contribution to these global objectives:

- **SDG 3 (Good Health and Well-being):** The proposed replacement of hazardous acids with safer deep eutectic solvents in the recovery process of antimony from effluents could potentially mitigate health risks associated with the handling of these dangerous chemicals.

- **SDG 6 (Clean Water and Sanitation):** The research contributes to this goal by exploring alternatives to strong acids, the use of which can lead to water acidification.

- **SDG 9 (Industry, Innovation, and Infrastructure):** The research introduces an innovative approach to the copper electrorefining process, potentially leading to more sustainable industrial practices.

- **SDG 12 (Responsible Consumption and Production):** The focus on the recovery of antimony and the exploration of green solvents aligns with this goal's emphasis on the environmentally sound management of chemicals and waste.

- **SDG 14 (Life Below Water):** Strong acids like HCl contribute to environmental acidification, lowering the pH of water bodies and impacting water health, which in turn affects living and growing conditions of life in the water. By addressing water acidification by replacing the strong acids, the research directly contributes to the protection of marine ecosystems.

Most of the SDGs are interconnected, and advancements in one area often leads to progress in others. Therefore, the impacts of this research could potentially extend to other SDGs as well.

Chapter 3

Materials & Methods

3.1. Preparation of Oxaline and the Antimony Dissolution

3.1.1. Preparation of the Deep Eutectic Solvent: Oxaline

The preparation of a DES involves multiple steps, beginning with the critical selection of suitable HBD and HBA components. As previously mentioned, a Type III DES called 'oxaline' was used in this research. Oxaline consists of choline chloride, which serves as the HBA, and oxalic acid, acting as the HBD. Both compounds are solid at room temperature, with melting points of 186 °C for oxalic acid and 302 °C for choline chloride.

After selecting the components, the next phase is mixing them. The solid compounds, choline chloride and oxalic acid, are combined in a specific molar ratio to form the eutectic composition. This ratio is determined by stoichiometric considerations to maximize hydrogen bonding interactions, ensuring that each molecule of choline chloride can effectively pair with molecules of oxalic acid. As shown in Figure 17, which illustrates the reaction mechanism for the formation of the DES, the hydrogen bonds between choline chloride and oxalic acid are depicted with dotted lines.

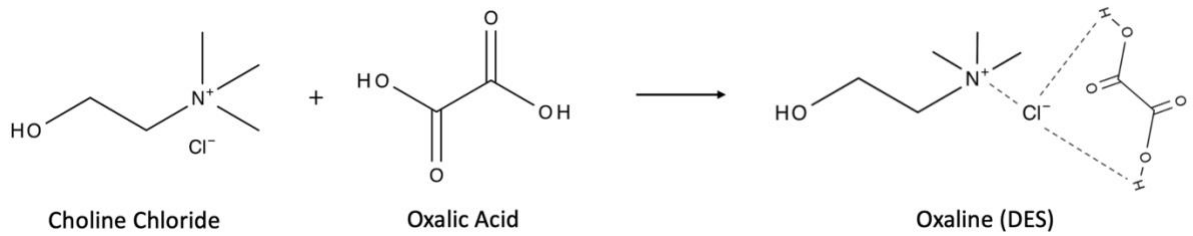

Figure 17: Reaction mechanism and hydrogen bonding interactions in the formation of oxaline (DES).

In this research, as in many other studies, a 1:1 molar ratio was used, representing an equal proportion of HBA to HBD. This ratio allows for optimal stability and the lowest melting point of the DES, compared to the individual components and other molar compositions.

The mixture of equimolar quantities was stirred while being heated to a temperature between 50 °C and 70 °C. Initially, the solid compounds were stirred manually until a portion of the mixture formed the DES, becoming liquid at this elevated temperature. Once a liquid phase is formed, magnetic stirring was applied to complete the DES formation until only a liquid phase remained. Depending on the required volume of DES, which in this research was approximately 80 mL, the solid compounds were added in multiple smaller (equimolar) steps. This method ensured faster DES formation, reduced manual labor, and resulted in a higher quality product.

3.1.2. Dissolution of Antimony in Oxaline

After preparing the eutectic solvent, antimony was added to the oxaline. Initially, Antimony(III)oxide (Sb_2O_3) was used, but due to unsatisfactory results, it was replaced with Antimony(III)chloride ($SbCl_3$) as the antimony source.

In this research, a 10 mM Sb solution was used for the experiments, meaning 10 millimoles of antimony are added per liter of oxaline solution. Depending on the antimony source, the required mass varied because of the difference in molar mass as well as the number of antimony atoms per molecule of the antimony source.

When using the oxide (Sb_2O_3), which has a molar mass of 291.52 g/mol and contains two Sb atoms per molecule, 1.457 g/L was required. For the chloride ($SbCl_3$), which has a molar mass of 228.12 g/mol and contains one Sb atom per molecule, 2.281 g/L was needed.

This amount was added to the oxaline in a single step once the eutectic solvent was fully formed and thereby completely in the liquid phase. After adding the antimony, the solution was briefly stirred manually before applying magnetic stirring while maintaining the temperature between 50 °C and 70 °C.

3.2. Dilution of Oxaline with HCl

For the analysis of antimony concentrations of the samples taking during the electrodeposition experiments, atomic absorption spectroscopy was used. This analytical technique is explained in Chapter 1, Section 1.8.1: ‘Working Principle of AAS’.

This technique, as described before, requires that the sample solution could be drawn through the capillary tube of the AAS before being nebulized. However, this was not possible due to the high viscosity of the samples. Additionally, the antimony concentration of the samples exceeded the measurement range of the AAS. Therefore, to lower the viscosity and bring the antimony concentration within the measurement range of the AAS, the samples were diluted in 0.3 M HCl. This ensures proper nebulization and accurate measurements.

Because oxaline with added antimony exhibited high viscosity, as will be discussed in detail in Chapter 4, Section 4.1.2: 'Dissolution of Antimony in Oxaline'. This high viscosity not only hindered the analysis with AAS but also interfered with the rotation of the magnetic stirring rod during the experiments, thereby limiting the results.
It was observed that adding small volumes of HCl significantly altered the physical properties of the previously prepared DES (with and without Sb), including lowering viscosity and increasing transparency. Therefore, for the additional experiment, oxaline was prepared and 10 mM antimony was added as described previously, followed by the addition of 10 % v/v of a 3 M HCl solution. A repeat experiment was then conducted to compare the results of the solutions with and without HCl.

3.3. Cyclic Voltammetry

3.3.1. Experimental Setup

The cyclic voltammetry experiments were conducted using a standard three-electrode cell as shown in Figure 18. The working electrode was a platinum disk embedded in Teflon, with an effective area of 0.071 cm^2. The reference electrode was a standard Ag/AgCl (3 M KCl) electrode, and the counter electrode was a platinum ring with an area of 1 cm^2.

The positioning of the electrodes is such that all three are submerged at an equal depth in the solution. The arrangement from left to right in Figure 18 is as follows: the working electrode, the reference electrode, and the counter electrode. Notably, the RE is placed between the WE and the CE but is situated closer to the WE. This strategic placement ensures consistent and accurate measurements during the experiments, with an intentional focus on the WE.

The experiment utilizes a jacketed electrochemical cell, which is connected to a temperature-controlled system for heating (or cooling) water. This allows for precise control over the temperature of the solution during the experiment.

A magnetic stirrer (without heating) was used. It features accurate rotation control, which allows for precise investigation of the effect of the rotation speed on the voltammograms. The electrodes were connected to an Autolab potentiostat/galvanostat, which was in turn connected to a computer.

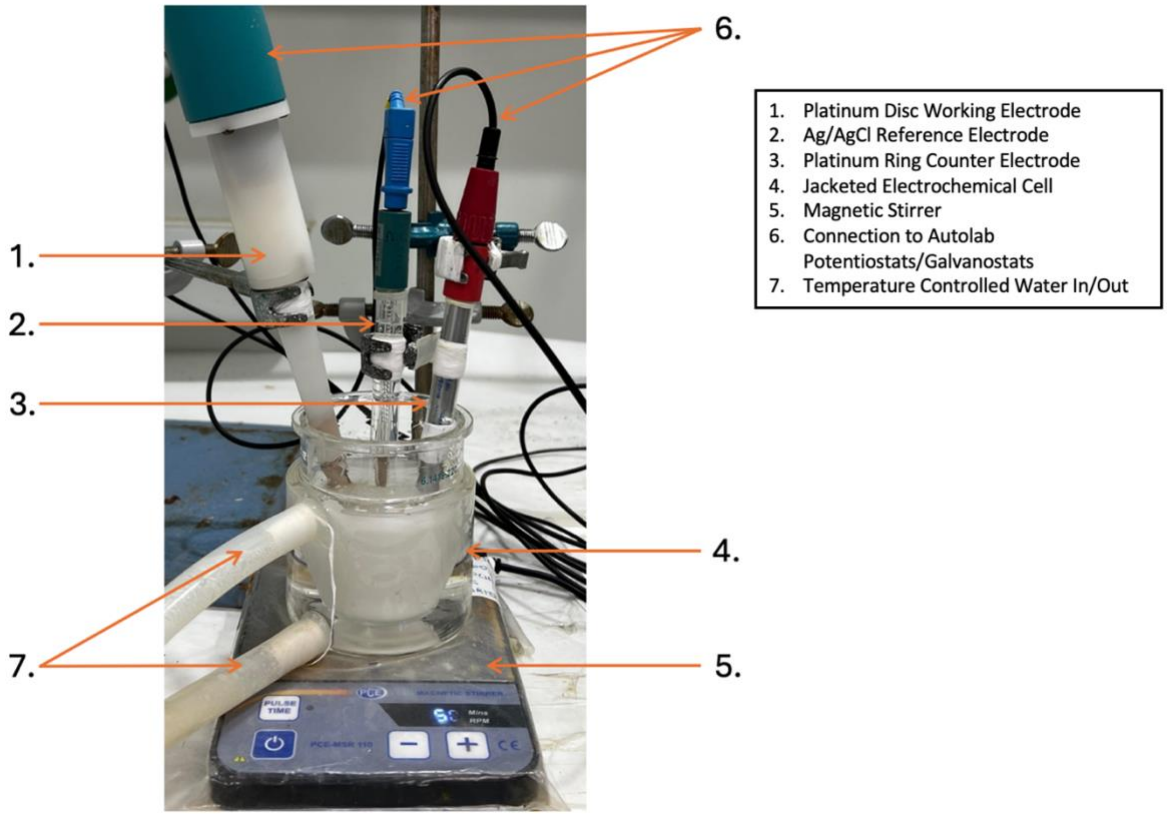

Figure 18: Cyclic Voltammogram – Experimental setup of the electrolytic cell for the recording of the cyclic voltammograms.

3.3.2. Experimental conditions

The cyclic experiments were conducted to study the system under controlled conditions. These conditions included a precisely controlled temperature of 80 °C, maintained using a jacketed electrochemical cell. The magnetic stirrer's rotation speed was set to 50 rpm, and the scan rate was set to 40 mV/s.

In each cyclic voltammogram experiment, the OCP was identified by allowing the electrode to equilibrate for a maximum duration of 60 seconds. To ensure consistency, multiple cycles or OCP passings (10 passings, 5 cycles) were performed in each experiment. Between each experiment, the electrode was thoroughly cleaned to maintain accuracy and reliability of the results.

A cyclic voltammetry experiment under these consistent conditions was conducted using an oxaline solution without antimony, intended as the blank to determine the solvent limit. Additionally, an experiment was conducted using an oxaline solution containing 10 mM Sb under the same conditions.

The specific conditions tested are summarized in Table 2.

Table 2: Cyclic voltammetry experimental parameters.

Parameter	*Values*
Temperature (°C)	80
Rotation Speed (rpm)	50
Scan Rate (mV/s)	40
Solution	Blank – oxaline (0 mM Sb) Oxaline (10 mM Sb)
Cycles *OCP passings*	5 cycles 10 OCP passings

3.4. Linear Sweep Voltammetry

3.4.1. Experimental Setup

As explained before, LSV focuses only on the analysis in one direction, corresponding to the reaction of interest. LSV is used when the material of the working electrode is susceptible to damage at either anodic or cathodic potentials. In this research, copper (Cu) is used as the working electrode (cathode), which can undergo oxidation and subsequent dissolution when scanned at anodic potentials. Therefore, when using the Cu-electrode, LSV is exclusively scanned over the cathodic potentials to prevent such degradation.

The configuration of LSV is based on a three-electrode setup, as shown in Figure 19, which presents the experimental setup for linear voltammetry. This setup includes several key components, with the copper (Cu) electrode serving as the WE. Copper was chosen for its cost-effectiveness and proven efficiency in the large-scale recovery of Sb.

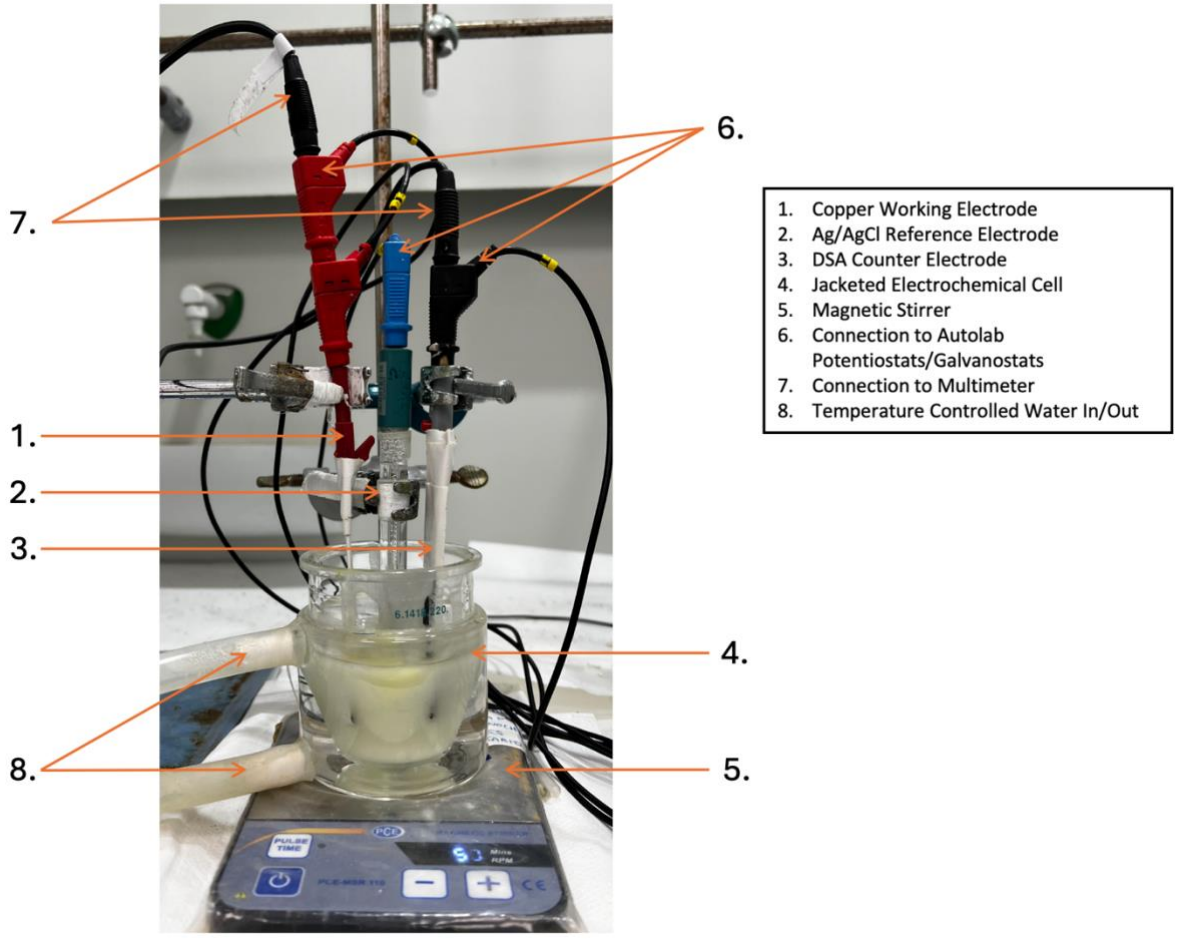

Figure 19: Linear Sweep Voltammetry – Experimental setup of the electrolytic cell for the recording of the Linear voltammograms.

The copper electrode used in this research for the linear sweep voltammetry as well as the electrodeposition experiments is shown in Figure 20. The electrode consists of a red alligator clamp, white insulating tape, and an exposed copper area.

The alligator clamp, along with a cable, connects the copper plate to the measurement device. The insulating tape is wrapped around the electrode to cover part of it, preventing unwanted contact between this part of the electrode and the electrolyte. The back of the electrode was completely covered by the tape, leaving only the area on the front of the electrode exposed. This exposed copper area, which measures 6 cm^2, is the part of the electrode that was in direct contact with the electrolyte during the experiments, where the reactions (reduction) occur.

Figure 20: Copper Working Electrode.

Similar to the CV – setup, the setup of the LSV also included an Ag/AgCl reference electrode that provided a stable reference potential, which was essential for measuring the potential of the working electrode.

As for the counter electrode, a Dimensionally Stable Anode (DSA), also known as a Mixed Metal Oxide (MMO) electrode, was used to maintain the charge balance of the system. This DSA electrode, shown in Figure 21, is made from titanium mesh and coated with a mixed metal oxide, specifically a mixture of ruthenium dioxide (RuO_2) and iridium dioxide (IrO_2) in a ratio of 0.70 to 0.30. This combination provides high stability and efficiency.

Figure 21: Mixed Metal Oxide - Mesh Counter Electrode, Dimensionally Stable Anode.

Apart from the different electrodes and the addition of a multimeter, the experimental setup remained practically the same as the CV setup. The three electrodes were immersed in the electrolyte to the same depth in the jacketed electrochemical cell, which contained the solution and a magnetic stirrer. The jacketed design allowed the temperature to be controlled and kept constant during the experiment.

LSV is particularly useful as a preparatory test for electrodeposition experiments. It can be conducted under the same conditions and with the same electrodes as the electrodeposition experiments, such as the copper electrode, which would oxidize at anodic potentials. The large electrode area and identical hydrodynamic conditions were maintained, making LSV an ideal precursor to electrodeposition.

3.4.2. Experimental Conditions

Experiments were conducted using an oxaline solution containing 10 mM Sb at two different temperatures, 60 °C and 80 °C. The rotation speed of the magnetic stirrer was set to 50 rpm. The OCP for these experiments was similar to CV, identified by allowing the electrode to equilibrate for a maximum duration of 60 seconds. The potential range extended from the OCP to -1.8 V. Between experiments, the electrode was thoroughly cleaned and sanded down to ensure accurate and reliable results.

3.5. Electrodeposition of Antimony

3.5.1. Experimental Setup

The experimental setup for the electrodeposition experiments (galvanostatic and potentiostatic) used the same three-electrode setup as the LSV experiments (Figure 19). Consisting of the copper working electrode (Figure 20), the Ag/AgCl reference electrode, and the MMO-mesh counter electrode (Figure 21).

3.5.2. Experimental Conditions of the Electrodeposition

For both the potentiostatic and galvanostatic experiments, the temperature was held constant at 80 °C using the precisely temperature-controlled, water-heated, jacketed electrochemical cell. The rotation speed of the magnetic stirrer was set to 50 rpm. The potential values applied during the electrodeposition conducted in potentiostatic mode, as well as the current density values applied in the galvanostatic experiments, were selected based on previous LSV curves.

The potential and current density values used in the subsequent potentiostatic and galvanostatic experiments are provided in Table 3. These values were carefully selected based on the previous LSV experiments, as previously discussed. More detailed explanations of these values can be found in the results and discussion Chapter 4, Section 4.4: ‘Electrodeposition of Antimony’.

Table 3: Potential and current density values used in the potentiostatic and galvanostatic electrodeposition experiments.

	Potential (mV)	*Current Density (mA/cm²)*
Pre-peak	-400	-0.18
Peak	-600	-0.62
Post-peak	-800	-1.27

3.5.3. Sampling

In both the potentiostatic and galvanostatic electrodeposition experiments, the duration was set to 3 hours. A sample was taken before the start of the experiment, and then during the first hour of the experiment, a sample was taken every 15 minutes. After the first hour, the sampling frequency was reduced to every 30 minutes. After the experiment, the solution was manually stirred to ensure it was homogeneous, and an 'end sample' was taken. Therefore, ten samples were taken during the 3-hour experiment, as outlined in Table 4.

Table 4: Sample taking time interval.

Sample nr.	**1**	**2**	**3**	**4**	**5**	**6**	**7**	**8**	**9**	**10**
Time (min)	0	15	30	45	60	90	120	150	180	END

For the sampling, 1 mL of solvent was taken from close to the WE with an adjustable micropipette. This 1 mL was then diluted to 50 mL with a 0.3 M HCl solution, so that the samples could be drawn through the capillary of the AAS, as previously discussed in Chapter 3, Section 3.2: 'Dilution of Oxaline with HCl'.

3.6. Spectroscopic Analysis

3.6.1. Experimental Setup

The experimental setup was designed to measure the concentration of antimony in samples using AAS. The centerpiece of the setup is the Perkin Elmer AAnalyst 100 Spectrophotometer, as depicted in Figure 22.

Figure 22: Atomic Absorption Spectrometer for Antimony measurements

For the measurement, a hollow cathode lamp specifically designed for antimony was employed, operating at a wavelength of 217.6 nm. The wavelength is a critical parameter in AAS, as it corresponds to the specific energy level transition of electrons in antimony atoms. By utilizing this particular wavelength, it ensured that the light absorption observed was attributable to the presence of antimony in the sample.

The spectral bandwidth was set at 0.2 nm. Spectral bandwidth indicates the range of wavelengths emitted by the lamp. A narrower bandwidth results in more monochromatic light, which improves the precision of the measurements.

The lamp operated at a current of 15 mA, which refers to the amount of electric charge flowing through the lamp.

The fuel-oxidizer ratio was maintained at 2:4 ethylene to air. This ratio affects the flame temperature, which in turn affects the atomization of the sample. Higher temperatures can lead to more complete atomization but may also cause the sample to decompose.

3.6.2. Calibration and Analysis of Antimony

Calibration is a crucial step that was performed every time before the samples were measured. This ensured an accurate quantitative analysis of Antimony present in the samples.

The calibration process for antimony began with the 'Preparation of Standard Solutions'. A series of standard solutions, each with a known concentration of antimony, were prepared. The antimony standard set used for the calibration of the AAS, with its corresponding concentrations in parts per million (ppm) is shown in Table 5.

Table 5: Antimony Standard Set for Calibration of the AAS.

Standard Solution nr.	**1**	**2**	**3**	**4**	**5**	**6**	**7**	**8**	**9**
Concentration Sb (ppm)	0	1	2	5	10	20	40	60	80

The standard set is prepared by diluting a 1000 mg/L standard solution with a 0.3 M HCl solution so that Sb is dissolved until the desired concentration was achieved.

Next, the absorbance of each standard solution in the set was measured using a spectrometer. According to the Lambert-Beer law, the absorbance is directly related to the concentration of antimony in the solution. The measured absorbance values were plotted against the known concentrations to create a calibration curve, as shown in Figure 23. This curve served as a reference for determining the concentration of antimony in unknown samples.

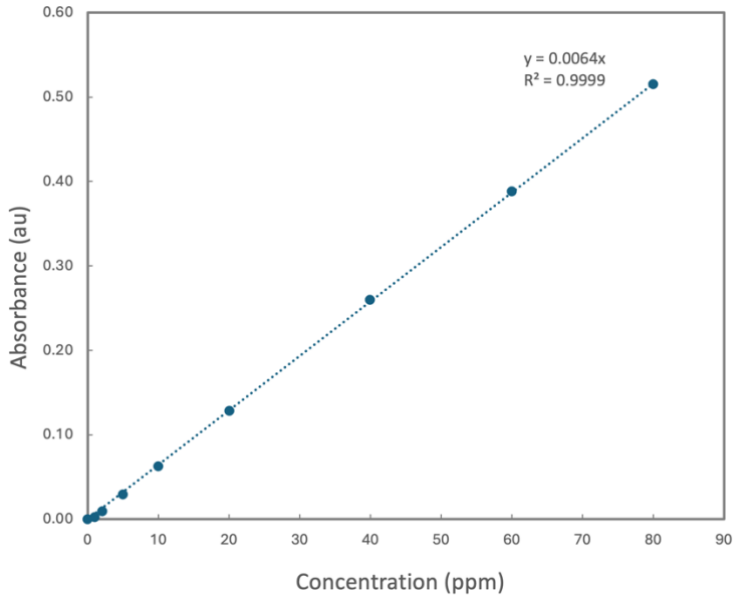

Figure 23: Example calibration curve of the atomic absorption spectrometer for the analysis of Sb.

As shown in the example calibration curve, the R^2 value (0.9999) of this method for measuring Sb is high, which indicates a strong correlation between the measured absorbance and the concentration. This means that the calibration curve for Sb can be used with high confidence to determine the concentration of antimony in unknown samples.

Chapter 4

Results & Discussion

4.1. DES preparation and Sb dissolution

As discussed in Chapter 3, Section 3.1.1: 'Preparation of the Deep Eutectic Solvent: Oxaline', the preparation of the eutectic solvent oxaline can be divided into multiple steps. The process began with the selection of suitable HBA and HBD components, which for oxaline are choline chloride and oxalic acid, respectively. The next step was the mixing phase, where the choline chloride and oxalic acid were combined in a specific molar ratio. This mixture was then heated and stirred to form the eutectic composition before adding the antimony.

4.1.1. Preparation of DES

This multistep preparation process, as carried out in this research, is illustrated in Figure 24.

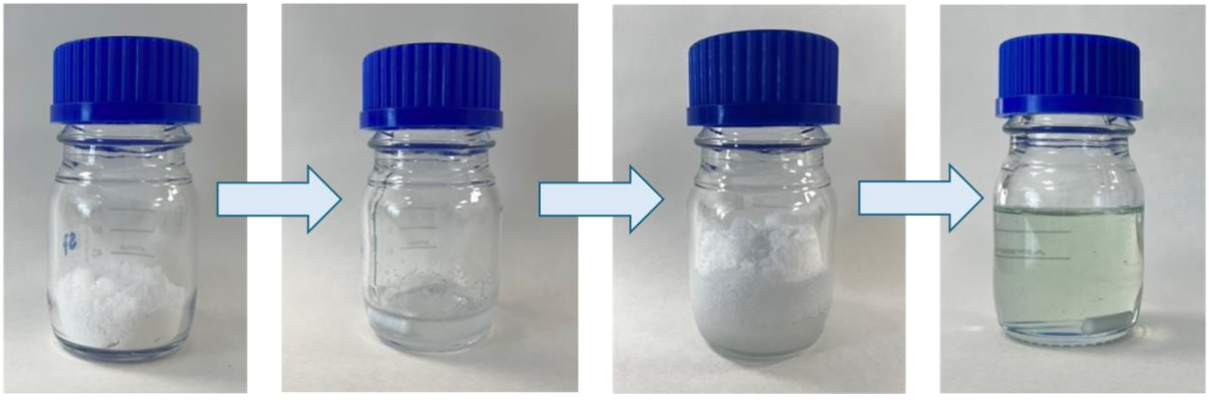

S1	S2	S3	S4
Initial quantities of choline chloride and oxalic acid	Formation of the deep eutectic solvent Oxaline (liquid)	Addition of more choline chloride and oxalic acid	Final volume of oxaline

Figure 24: Preparation of Oxaline.

In the first step (S1), the container was cleaned and preheated, and equimolar quantities of the solid compounds choline chloride and oxalic acid were added. At this point in the process, automatic stirring was not possible due to the presence of only solid substances and the

formation of large, hard solid pieces. Therefore, the mixture had to be manually mixed and broken down while being further heated to 50 °C. Gradually, the eutectic solvent began to form, and the initial solid mixture slowly transitioned into a liquid. Once sufficient liquid phase was formed, as can be seen in S2 of Figure 24, automatic stirring could be applied.

In the following step (S3), larger equimolar quantities of choline chloride and oxalic acid were added to the eutectic liquid formed in S2. The mixture was again manually mixed for approximately 10 minutes until automatic stirring could be applied. This process was repeated four times to achieve the required volume for the subsequent test.

By the end of the DES preparation, a clear homogeneous mixture with a volume of approximately 80 mL was obtained, as depicted in S4 of Figure 24.

Different mixing/weighing steps were investigated to identify the quickest and least labor-intensive process. These ranged from adding the entire desired mass at once to adding it in 2, 3, or even 4 increments. All the investigated methods can be found in the 'Appendices',

The process that required the least amount of manual mixing and breaking of larger solid pieces is shown in Table 6. This process involved 4 steps, with each step increasing in mass. The quickest process was found to be the 3-step process and is shown in Table 7, but it required more manual mixing, although not as much as in the 1 or 2-step processes.

Table 6: Mixing steps in the preparation of the DES with the least amount of manual mixing required.

	Oxalic Acid mass (g)	*Choline Chloride mass (g)*
1	6.7881	10.5112
2	9.9818	15.4487
3	10.0789	15.6435
4	12.0087	18.6636

Table 7: Mixing steps in the preparation of the DES, fastest process.

	Oxalic Acid mass (g)	*Choline Chloride mass (g)*
1	13.5324	21.6889
2	13.1940	20.6159
3	14.1781	21.1193

The kinematic viscosity of the oxaline solution was measured using a Fenske viscometer across different temperatures, revealing a decreasing trend with rising temperatures. At 60 °C, the viscosity was recorded at 1100 mm^2/s. As the temperature increased to 70 °C, the viscosity dropped significantly to 690 mm^2/s. Further heating to 80 °C resulted in a viscosity of 580 mm^2/s.

4.1.2. Dissolution of Antimony in Oxaline

After the preparation of the eutectic solvent, the next step involved the addition of antimony to the oxaline. Antimony was carefully added to the DES under controlled conditions. Initially, a 10 mM solution of antimony, added in the form of Antimony(III)oxide (Sb2O3), was utilized in this research. However, the voltammetry experiments conducted with this oxide did not yield satisfactory results, as no reduction peak was observed. To improve the results, the concentration of Sb was increased to 20 mM, but the outcomes remained unsatisfactory. The solubility of oxide in the DES was found to be poor, which might have contributed to these unsatisfactory results.

Consequently, a shift was made to use Antimony(III)chloride ($SbCl_3$) instead of the oxide. Although the chloride is more soluble than the oxide, it still requires a considerable amount of time to dissolve completely. The dissolution process is shown in Figure 25, were S1 is the DES solution without Sb (S4 of Figure 24), S2 is the solution after Sb was added and manually stirred for 2 minutes, and finally the S3 shows the solution after the Sb dissolution was complete.

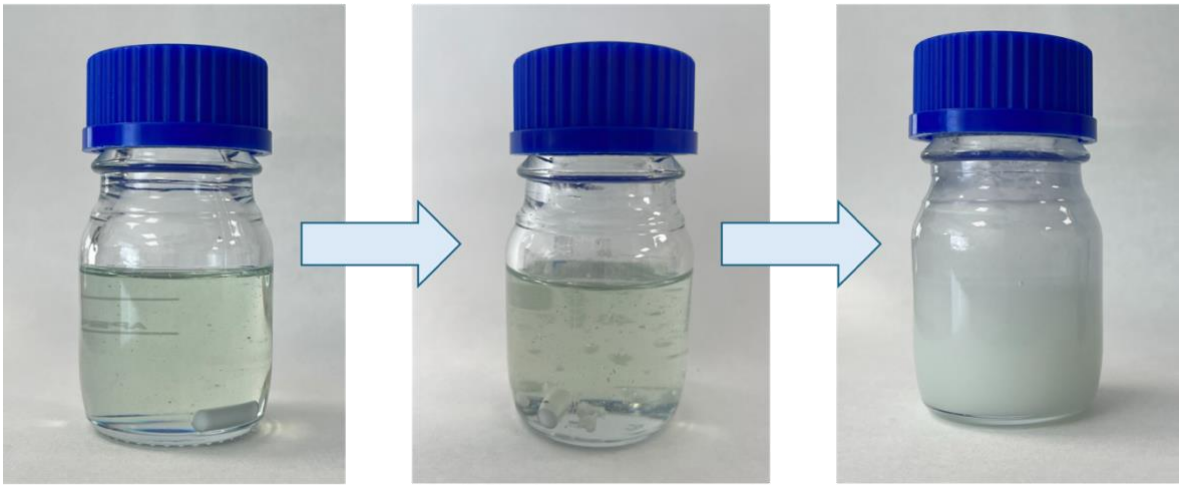

Figure 25: Dissolution of Antimony(III)chloride in Oxaline.

As shown in Figure 25, the addition of antimony causes the solution to become opaque, significantly reducing its transparency. There was also a notable increase in viscosity both when the solution was heated and when it was cooled to room temperature, compared to the solvent without Sb when heated and at room temperature, respectively. At room temperature, the solution without Sb was highly viscous, whereas the mixture with Sb solidified.

4.2. Cyclic Voltammetry

4.2.1. Voltammogram Cycles and OCP - determination

The OCP is identified by allowing the electrode to equilibrate for a maximum duration of 60 seconds. This stabilization indicates that the electrode has reached a steady-state condition, which corresponds to the OCP where the net current is zero. As shown in Figure 26, the OCP is marked by the dashed green line at -0.225 V. This value indicates the potential at which the system's electrochemical reactions are at equilibrium.

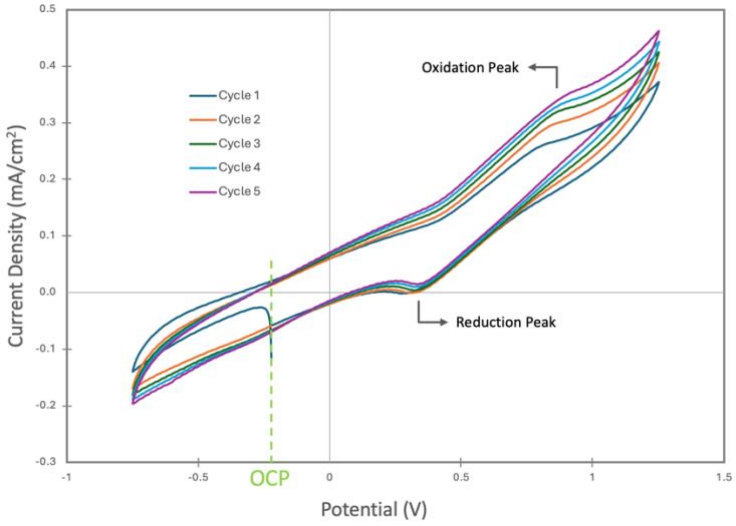

Figure 26: Cyclic Voltammogram of DES with 10 mM Sb at 80 °C, 40 mV/s and 50 rpm, showing multiple OCP passings (10 Passings, 5 Cycles).

In the presented voltammogram, and in all the conducted CV experiments, ten OCP passings were conducted, resulting in five complete cycles. The multiple OCP passings serve to demonstrate the reproducibility and stability of the electrochemical system. Each cycle shows distinct oxidation and reduction peaks, which are characteristic of the redox-active species involved in the reactions.

The figure illustrates how each cycle's peaks align closely with one another, indicating consistent electrochemical behavior across multiple cycles. This consistency is crucial for validating the stability and reproducibility of the system under investigation.

The increase in peak current densities with successive cycles suggests an improvement in the electrochemical reaction kinetics, likely due to the activation and stabilization of the electrode surface. This phenomenon is commonly observed in cyclic voltammetry and indicates the system's adaptability and potential for enhanced performance over multiple cycles [10]. The progressive rise in peak currents may also imply a growing accessibility of the redox-active sites or a reduction in resistance at the electrode interface.

4.2.2. Impact of Antimony on the voltammograms of Oxaline

The CV experiment comparing oxaline solutions with and without antimony is presented in Figure 27. Both experiments were conducted under identical conditions: temperature at 80 °C, stirring at a rotation speed of 50 rpm, and a scan rate of 40 mV/s. These consistent experimental conditions ensured that the observed differences in the voltammograms are attributable to the presence of Sb, allowing for a direct comparison of the two scenarios.

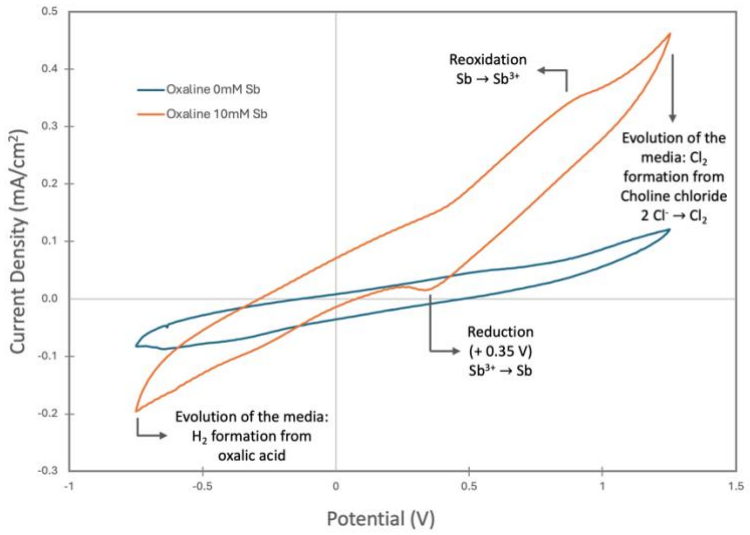

Figure 27: Cyclic Voltammogram comparison of Oxaline with (10 mM) and without antimony.

The CV curve for oxaline without antimony (0 mM Sb) is represented by the blue line. This voltammogram serves as the baseline, depicting the electrochemical behavior of the oxaline solution in the absence of Sb. The observed current density is relatively low, indicating limited electrochemical activity within the potential range investigated. As can be seen the curve is quite flat as compared to the voltammogram obtained with Sb.

The key features of this voltammogram include:

- A small oxidation peak around 0.6 V, suggesting minimal oxidation activity in the oxaline solution.

- A corresponding reduction peak observed around -0.3 V, indicating some degree of reversible electrochemical reaction.

These peaks are not pronounced, signifying that the oxaline solution alone does not exhibit significant redox activity within the scanned potential range.

The CV curve for oxaline with 10 mM Sb is shown by the orange line. The addition of Sb significantly alters the electrochemical behavior of the oxaline solution, as evidenced by the notable changes in the voltammogram.

The key features of this voltammogram include:

- A substantial oxidation peak current density observed around 0.9 V, indicating a pronounced oxidation process facilitated by the presence of Sb in the solution.
- A notable reduction peak occurring around 0.35 V, suggesting enhanced reversible redox reactions compared to the solution without Sb.

Given that the working electrode is Platinum (Pt), the interpretation of the reduction peak at a positive potential (0.35 V) in the cyclic voltammogram for oxaline with 10 mM Sb can be explained as follows. Platinum is renowned for its excellent catalytic properties and wide potential window, significantly influencing the electrochemical behavior of species in solution. The reduction peak at 0.35 V indicates that the Sb species (Sb(V) or Sb(III)) are being reduced at a relatively positive potential, suggesting that the platinum electrode effectively facilitates this reduction process.

The catalytic properties of platinum lower the activation energy for the reduction of Sb species, resulting in the observed shift to a more positive potential. Additionally, the strong interaction between Sb species and the Pt surface enhances the electron transfer processes, making the reduction more favorable. Surface adsorption effects on the platinum electrode can further modify the local electrochemical environment, stabilizing the Sb species and facilitating their reduction at higher potentials. The rapid electron transfer kinetics on platinum also contribute to the efficient reduction process observed at 0.35 V [11].

When the potential is reversed, a reoxidation peak can be observed at +0.9 V. This indicates that the deposited Sb is being reoxidized to Sb(III) and/or Sb(V). As the potentials reach extreme values, evolution in the media can be observed, at potentials exceeding +1.20 V, Cl_2 formation occurs due to the oxidation of Cl^- ions originating from chlorine chloride. At the other extreme, at potentials lower than -0.70 V, H_2 formation occurs as a result of the hydrogen evolution reaction (reduction) due to oxalic acid.

The comparison between the two voltammograms clearly demonstrates the impact of Sb on the electrochemical behavior of the oxaline solution. The presence of Sb significantly enhances the electrochemical activity, as evidenced by the increased current densities and more pronounced redox peaks.

4.3. Linear Sweep Voltammetry

The subsequent LSV experiments only focuses on the analysis in one direction, which in this research is the reduction of Sb. This is, as previously discussed, due to the material used for the working electrode, which is copper. Since copper can undergo oxidation and subsequent dissolution, only the reduction part of the LSV is analyzed.

The combined Oxaline with 10 mM Sb at 60 °C and 80 °C, presented in Figure 28, reveals important differences in the electrochemical behavior of the system at these two temperatures. The sweeps were performed from the OCP at -0.27 V to -1.8 V, with the zone of interest shown in the figure between -0.3 V and -1.2 V.

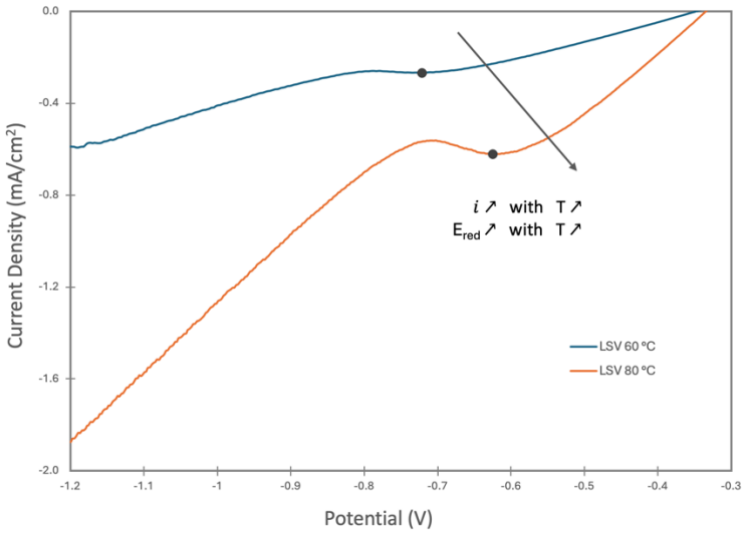

Figure 28: Linear Sweep Voltammogram temperature comparison of Oxaline with 10 mM Sb at 80 °C.

The key features of the voltammogram at 60 °C include:

- The onset of reduction is observed around -0.6 V.
- The reduction peak occurs at -0.72 V with a corresponding current density of approximately -0.26 mA/cm².
- Idem: After the peak, a plateau or slight decrease in the current density indicates a diffusion-controlled regime.
- Idem: Beyond the plateau, starting around -0.9 V, there is a sharp increase in current density, marking the onset of hydrogen formation.

The key features of the voltammogram at 80 °C include [30]:

- The onset of reduction is observed around -0.5 V.
- The reduction peak occurs at approximately -0.6 V. This is the maximum current density (cathodic current) associated with the reduction process. It corresponds to the most favorable reduction potential for the analyte. The corresponding current density of approximately -0.6 mA/cm².

- After the peak, a plateau or slight decrease (in absolute value) of the current density indicates a diffusion-controlled regime.

- Beyond the plateau, starting around -0.8 V, there is again an increase in current density (absolute values), marking the onset of hydrogen formation.

4.3.1.1. Comparison and Discussion

At 80 °C, the onset of Sb reduction occurs at a lower potential (absolute) value (-0.5 V) compared to 60 °C (-0.6 V). This suggests that higher temperatures lower the activation energy for the reduction process, making it easier for Sb ions to reduce at less negative potentials [12].

At both temperatures, a reduction peak is observed. For the lower temperature at 60 °C, this occurs at -0.72 V, which is at a more negative potential than at 80 °C, where it occurs at -0.6 V. This shift indicates that at lower temperatures, a higher overpotential is required to drive the reduction process due to slower reaction kinetics and reduced ion mobility.

The peak current density at these reduction potentials represents the limiting current density (i_L), where mass transfer limitations from the dissolved Sb to the electrode surface prevent higher current densities from being recorded. The i_L at 80 °C (-0.6 mA/cm²) is significantly higher than at 60 °C (-0.26 mA/cm²), indicating a more efficient reduction process at higher temperatures. This higher efficiency can be attributed to enhanced ion mobility and faster reaction kinetics at elevated temperatures. At 80 °C, the increased temperature reduces the viscosity of the solution, improving ion transport to the electrode surface and thereby increasing the rate of Sb ion reduction.

After reaching the peak, there is a plateau or a slight decrease in the absolute value of the current density observed in both voltammograms. This decrease after the reduction peak indicates that the system has transitioned from being kinetically controlled to being diffusion-controlled. In other words, the rate of Sb ion reduction is now limited by the rate at which Sb ions can diffuse from the bulk solution to the electrode surface.

This behavior confirms that the reduction rate is controlled by the diffusion of Sb species to the electrode surface. The plateau suggests that the electrode surface is fully utilized for the reduction process, and any further increase in the applied potential does not significantly enhance the reduction rate due to mass transfer limitations.

Hydrogen evolution begins at a less negative potential at 80 °C (-0.8 V) compared to 60 °C (-0.9 V), indicating that at higher temperatures, the overpotential for hydrogen evolution is reduced. This suggests that at 80 °C, hydrogen formation competes more closely with Sb

reduction, whereas at 60 °C, the Sb reduction process occurs for a longer range of potentials before hydrogen evolution becomes significant.

Overall, the combined LSV curves demonstrate that increasing the temperature enhances the reduction efficiency of Sb in Oxaline, with higher current densities and earlier onset of reduction and hydrogen evolution. The reduction potential observed in previous CV experiments using platinum (Pt) as the working electrode differed from the values obtained when copper was used. As explained in Chapter 4, Section 4.2.2: 'Impact of Antimony on the voltammograms of Oxaline', the reduction potential values with copper in LSV experiments were higher in absolute terms than those with platinum in the CV experiments.

4.4. Electrodeposition of Antimony

4.4.1. Potentiostatic Electrodeposition

In this section, the potentiostatic electrodeposition of antimony is discussed. All experiments were conducted under controlled and consistent conditions to ensure the reliability and reproducibility of the results. This means that for each experiment, a new solution was prepared, and the same electrode was used. The electrode was cleaned and sanded down to the same grit each time. The temperature was maintained at 80 °C, and the rotation speed of the electrode was set to 50 rpm.

The potential values applied in the potentiostatic electrodepositions were determined from the linear voltammograms shown in Figure 29. This figure depicts the LSV obtained for Oxaline with 10 mM Sb at 80 °C and a rotation speed of 50 rpm, with the potentials and currents relevant to the electrodeposition studies indicated with dashed lines.

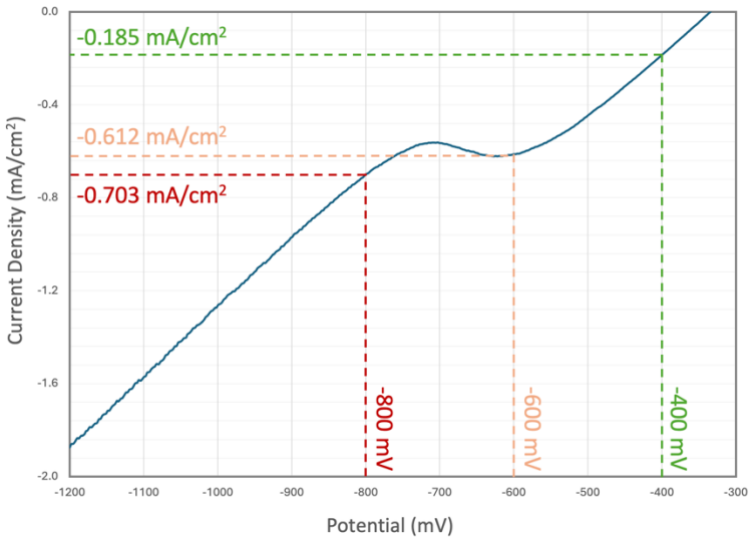

Figure 29: LSV of Oxaline with 10 mM Sb at 80 °C:
Potentials and Currents for Potentiostatic and Galvanostatic Electrodeposition Experiments.

Three potentials were chosen to study their effects on the reduction process:

- **-400 mV:** Before the reduction peak, at a less negative potential than the reduction peak potential.
- **-600 mV:** At the reduction peak.
- **-800 mV:** After the reduction peak, at a more negative potential than the reduction peak potential.

These specific potentials help in understanding the behavior of antimony deposition under different electrochemical conditions.

4.4.1.1. Potentiostatic electrodeposition at -400 mV

This first potentiostatic experiment, conducted at the least cathodic potential evaluated, is presented in Figure 30, which shows the current density over time during the potentiostatic electrodeposition of antimony at a potential of -400 mV. The experiment was conducted for a duration of 3 hours, during which multiple samples were taken.

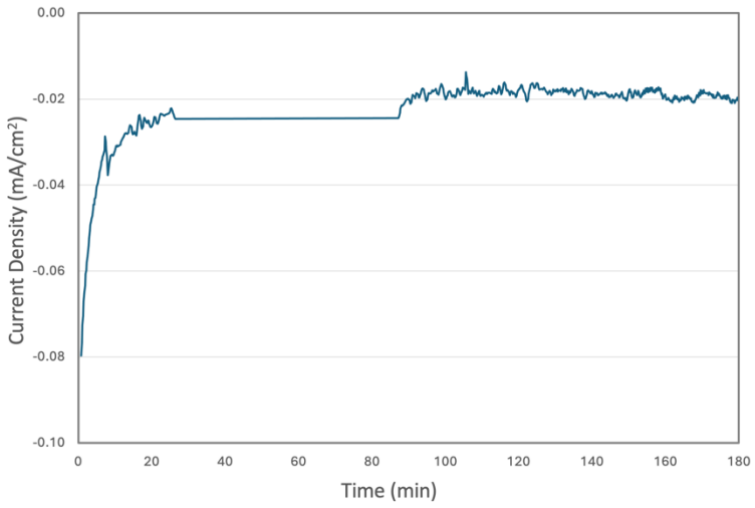

Figure 30: Potentiostatic Electrodeposition of Oxaline with 10 mM Sb at a potential of -400 mV.

The phenomenon observed in the potentiostatic electrodeposition of antimony in Figure 30, where the current density initially exhibits a rapid decrease in absolute value before stabilizing at around -0.02 mA/cm², can be explained by the electrochemical processes occurring at the electrode surface. Specifically, this involves the reduction of antimony ions (Sb^{3+}) from the electrolyte to metallic antimony (Sb^0) at the electrode surface. The reduction reaction can be represented as follows:

$$Sb^{3+} + 3e^- \rightarrow Sb^0 \quad (9)$$

At the beginning of the potentiostatic electrodeposition process, the applied potential (-400 mV in this case) is sufficient to initiate the reduction of Sb^{3+} ions from the Oxaline solution onto the electrode surface. Initially, there are many available active sites on the electrode surface, and the concentration of Sb^{3+} ions near the electrode is relatively high. This results in a high rate of reduction reactions, leading to a high current density (in absolute terms).

As the electrodeposition progresses, the available active sites on the electrode surface start to get occupied by deposited Sb^0. The concentration of Sb^{3+} ions near the electrode surface decreases due to the reduction reactions, leading to a phenomenon known as concentration polarization. Additionally, the diffusion layer (a region where the concentration of ions is depleted) starts to form near the electrode surface. These factors result in a rapid decrease in absolute value of the current density as the rate of reduction reactions slows down.

After the initial rapid decrease in absolute value, the system reaches a steady-state condition where the rate of Sb^{3+} ion reduction is balanced by the rate of mass transport of Sb^{3+} ions to the electrode surface. The current density stabilizes around a lower value (approximately -0.02 mA/cm²), which reflects the steady-state rate of the electrodeposition process. At this point, the electrode surface is partially covered by the deposited Sb, and the growth rate is now limited by the diffusion of Sb^{3+} ions to the electrode surface.

The fluctuations observed in the current density during the deposition process can be attributed to several factors, including slight changes in the electrode surface morphology, variations in the local concentration of antimony ions, or minor disturbances in the electrolyte flow. Although most of the fluctuations are due to these variable factors, the most severe fluctuations are due to the sample taking. This can be clearly observed at the 15-minute mark, when the first sample (after the initial sample) was taken, showing a disturbance in the curve. These fluctuations due to minor changes and sample taking are typically small (compared to the experiment) and do not significantly affect the overall deposition process. Additionally, there was an instrument malfunction during the experiment. Although not ideal, this had no real implication on the results of the experiment.

The choice of this less negative potential is aimed at studying the early stages of deposition, where nucleation dominates and the formation of a uniform seed layer is critical for subsequent growth.

4.4.1.2. Potentiostatic electrodeposition at -600 mV

This LSV of the second potentiostatic experiment, conducted at the reduction peak potential of -600 mV, is presented in Figure 31, which shows the current density over time during the potentiostatic electrodeposition of antimony. The experiment was again conducted for a duration of 3 hours, during which multiple samples were taken.

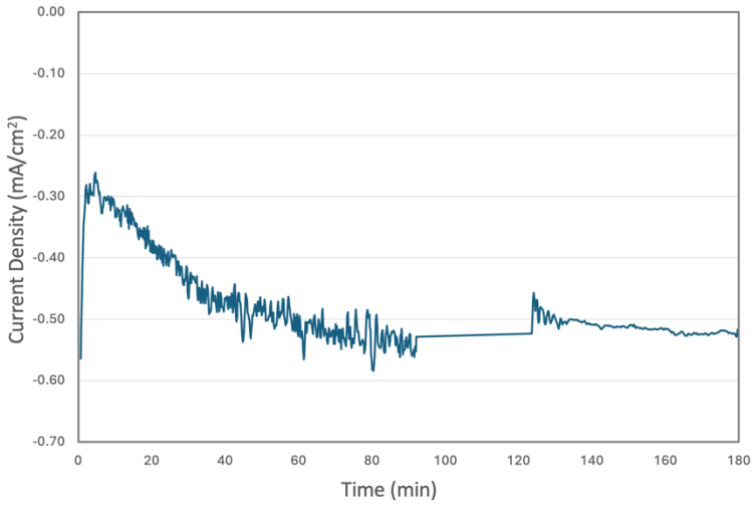

Figure 31: Potentiostatic Electrodeposition of Oxaline with 10 mM Sb at a potential of -600 mV.

The current density initially exhibited a rapid decrease in absolute value, from -0.63 to around -0.3 mA/cm², reaching a minimum peak value of -0.265 mA/cm². This is followed by a gradual increase in current density, stabilizing around -0.51 mA/cm². This behavior can be attributed to the electrochemical nucleation and growth processes on the electrode surface and the ion transport to the electrode [31].

The initial current density measurement is significantly higher at -600 mV (-0.63 mA/cm²) compared to -400 mV (-0.08 mA/cm²), indicating a higher nucleation/reduction rate due to the more negative potential, which enhances the reduction kinetics of Sb^{3+} ions.

At the beginning of the electrodeposition process, an initial rapid decrease in the absolute value of current density can be verified. This rapid decrease can be explained by two factors:

- The initial stage involves the charging of the electric double layer at the electrode interface. The electric double layer consists of a layer of charged particles (ions) adsorbed on the electrode surface and a layer of counter-ions in the solution adjacent to the electrode. As the double layer charges, the current density decreases.

- The high reduction rate of Sb^{3+} ions to Sb at the reduction peak potential initially consumes a large number of ions near the electrode surface. The applied potential of -600 mV provides a strong driving force for the reduction reaction, causing a high initial current density as the Sb^{3+} ions are rapidly reduced on the electrode surface.

After the initial rapid decrease and appearance of a minimum peak of -0.28 mA/cm², the current density begins to gradually increase before stabilizing at around -0.51 mA/cm². This gradual increase can be explained by several factors [10]:

- After the initial rapid reduction, nucleation of antimony atoms begins on the electrode surface, forming small clusters or nuclei of Sb^0. As these nuclei grow, they alter the

surface characteristics and increase the overall surface area available for the reduction reaction. This increased surface area allows more Sb^{3+} ions to be reduced simultaneously, leading to a gradual increase in current density.

- During the electrodeposition process, localized concentration gradients of Sb^{3+} ions can be formed near the electrode surface. As the system adjusts to these gradients, the current density increases as more ions are transported to the electrode surface.

After the gradual increase phase, the system eventually reaches a steady state where the current density stabilizes. This continuous deposition phase is characterized by the steady growth of the antimony layer on the electrode surface. The steady-state current density indicates the ongoing deposition of Sb^0 and remains relatively stable.

The stabilization period at -600 mV appears to be more prolonged and less stable compared to -400 mV. However, the steady-state current density of around -0.51 mA/cm² is higher than what was observed at -400 mV. This reflects the higher driving force for antimony ion reduction at the more negative potential, resulting in a higher deposition rate [10].

Analogous to the previous experiment, the fluctuations observed in the current density are primarily due to sample taking. Additionally, there was a noticeable instrument malfunction around minute 91, causing a temporary fluctuation. Despite these issues, the overall trend of the deposition process remained consistent.

4.4.1.3. Potentiostatic electrodeposition at -800 mV

When the potentiostatic electrodeposition is performed at a more negative potential than the reduction potential, specifically -800 mV as shown in Figure 32, several observations can be made. The experiment was, like the other experiments, conducted for a duration of 3 hours, during which multiple samples were taken.

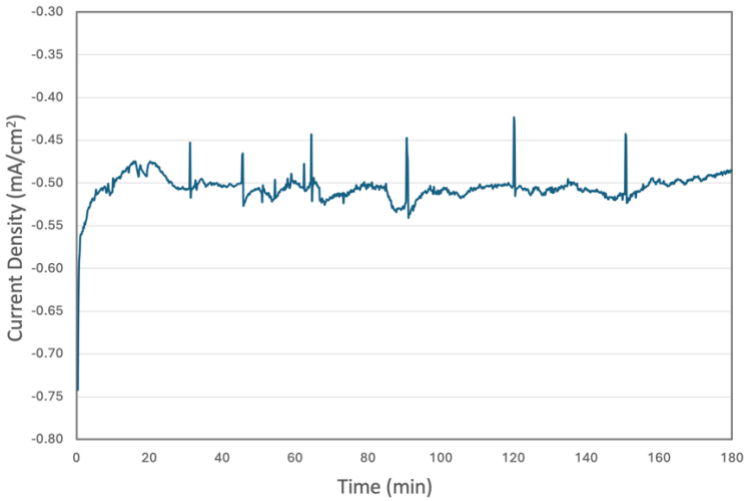

Figure 32: Potentiostatic Electrodeposition of Oxaline with 10 mM Sb at a potential of -800 mV.

The graph progresses similarly to that at -400 mV (Figure 30) with an initial rapid decrease (absolute value) in current density followed by the attainment of a steady-state. However, at -800 mV, both the initial current density and the steady state current density are significantly higher in absolute value compared to the process at -400 mV and thereby similar to the one at -600 mV (Figure 31).

At -800 mV, the initial current density is much higher (-0.74 mA/cm²) compared to the initial current density at -400 mV (-0.08 mA/cm²). This is because the more negative potential increases the driving force for the reduction reaction, leading to a higher rate of Sb^{3+} ion reduction to Sb^{0}.

The steady-state current density at -800 mV is also higher (approximately -0.50 mA/cm²) compared to the steady-state current density at -400 mV. This indicates that at -800 mV, even after the initial rapid decrease, the reduction reaction continues at a higher rate due to the increased driving force. At all the three measured potentials, the growth rate eventually becomes limited by the diffusion of Sb^{3+} ions to the electrode surface. However, the higher potential at -600 and -800 mV leads to a higher steady-state current density because the increased driving force for reduction can sustain a higher rate of Sb^{3+} ion reduction, despite the diffusion limitation. Ions may also be transported by migration due to the imposed electric field. So, transport may also improve a bit with higher potential.

The fluctuations in current density can be observed throughout the electrodeposition process, which are more pronounced at -800 mV when compared to those at -400 mV, but less pronounced than at -600 mV. As mentioned previously, such fluctuations may be attributed to the dynamic nature of the electrodeposition process, where localized changes in ion concentration, surface morphology, and nucleation sites can lead to transient variations in current density. While it was somewhat observable in the first experiment at -400 mV, the sample-taking disturbances are much more pronounced this time. Every time a sample was taken, the electrochemical environment was momentarily disturbed, leading to a noticeable fluctuation at that moment, which can be clearly seen at minute marks of 30, 45, 60, 90, 120, and 150. Despite these fluctuations, the overall trend of the deposition process remains consistent.

4.4.1.4. Potentiostatic electrodeposition Summary Graph

The graph in Figure 33 shows the LSV represented by the blue curve, alongside three steady-state current density values (red dots) obtained from potentiostatic electrodeposition over a duration of 3 hours at different potentials.

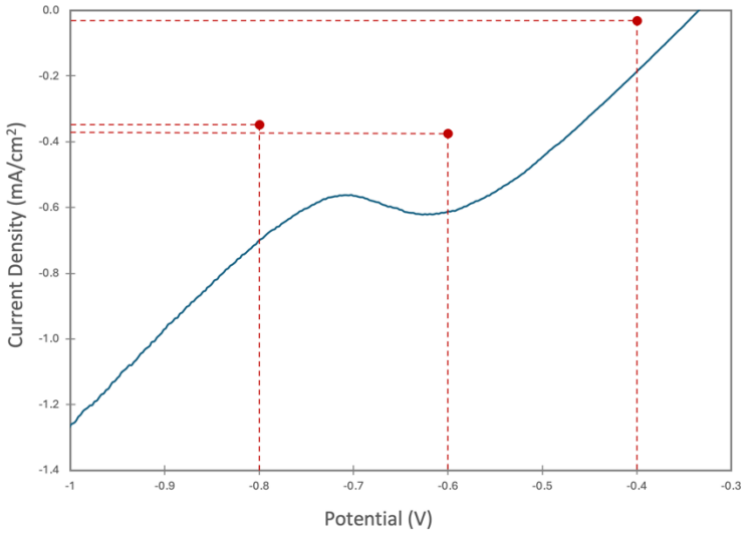

Figure 33: Steady-state values (red dots) of the current density obtained by potentiostatic electrodeposition, together with the LSV at 80 °C represented by the blue curve.

The steady-state values (red dots) are close to the LSV results (blue curve) but exhibit a lower current density. This difference can be attributed to several factors inherent in long-term potentiostatic electrodeposition experiments. Over extended periods, diffusion limitations become more pronounced as the concentration gradients of reactive species at the electrode surface deplete more significantly compared to the shorter time scales of LSV measurements.

4.4.1.5. Potentiostatic electrodeposition at -600 mV with HCl

As discussed previously, adding HCl to the oxaline solution significantly reduces its viscosity. This decrease in viscosity potentially lowers the mass transport limitation of the solution, enhancing its overall performance. To further investigate this effect, an additional LSV experiment was conducted at -600 mV.

The LSV curve of the potentiostatic experiment conducted at -600 mV with a solution containing 10 % v/v 3 M HCl is presented in Figure 34. The shape of the current density curve is similar to the previous experiment at -600 mV without HCl (Figure 31). However, several notable differences and additional observations were verified due to the presence of 3M HCl in the solution:

Initially, there is a very short and rapid decrease in the absolute value of current density from -1.68 to -1.22 mA/cm². This rapid initial decrease can be attributed to the same factors as before: the charging of the electric double layer and the high reduction rate of Sb^{3+} ions to Sb^{0} at the reduction peak potential.

Following the rapid initial decrease, the current density begins to gradually increase. The duration of this increase (stabilization period) is much shorter compared to the experiment without HCl.

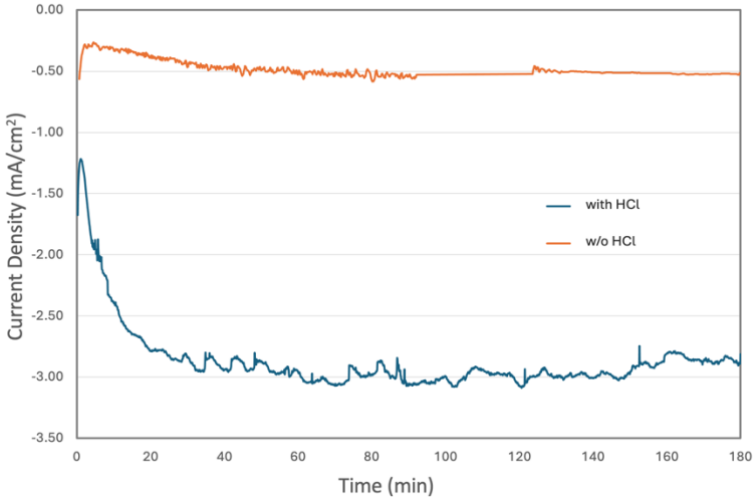

Figure 34: Potentiostatic Electrodeposition of Oxaline (10 mM Sb) with 10 % v/v 3M HCl (Blue line) and without HCl (Orange line) both at a potential of -600 mV.

The steady-state current density stabilizes around -3.0 mA/cm², which is significantly higher than in the previous experiment at -600 mV without HCl (-0.51 mA/cm²). Additionally, the initial current density is significantly higher, at -1.68 mA/cm² compared to -0.63 mA/cm² for the experiment without HCl.

4.4.1.6. Impact of HCl

Enhanced Ionic Conductivity

When HCl dissociates, H^+ and Cl^- ions are released. These ions increase the overall ionic strength of the solution [41], which reduces the electrical resistance and allows for more efficient current flow. The higher ionic strength facilitates better mass transport of Sb^{3+} ions from the bulk solution to the electrode surface because the movement of ions in the solution is less hindered by electrical resistance, allowing them to reach the electrode surface more readily.

Decreased Viscosity

The addition of HCl to the solution lowers its viscosity. A less viscous solution enables ions to move more freely and rapidly, reducing the diffusion layer thickness and enhancing ion transport. With reduced viscosity, Sb^{3+} ions can migrate more quickly towards the electrode surface, accelerating the rate at which they are reduced to Sb^0 and leading to a faster attainment of steady-state current density [42].

In addition, the presence of HCl may buffer the pH of the solution, maintaining a more stable environment for the reduction reactions. HCl can also affect the surface properties of the electrode, potentially increasing the number of active sites for nucleation and growth of Sb. This results in a higher surface area available for the electrochemical reaction. Increased nucleation can contribute to higher and more stable current densities during the steady-state phase, as more Sb^{3+} ions are continuously reduced at these sites.

4.4.2. Galvanostatic Electrodeposition

4.4.2.1. Galvanostatic electrodeposition at -1.27 mA/cm²

The galvanostatic electrodeposition of oxaline was conducted using a solution containing 10 mM Sb at a constant current of -1.27 mA/cm². The electrode potential (V) was monitored over a period of 180 minutes to observe the deposition process (Figure 35).

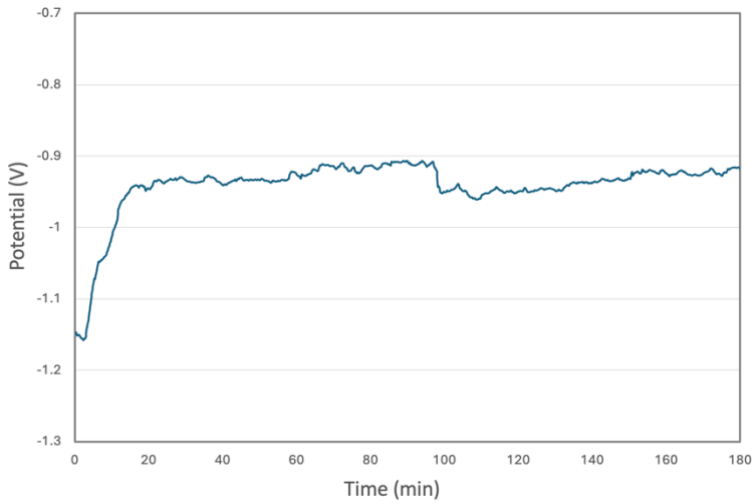

Figure 35: Galvanostatic Electrodeposition of Oxaline with 10 mM Sb at a current of -1.27 mA/cm².

Figure 35 shows the potential behavior during the electrodeposition of antimony from the oxaline solution with 10 mM Sb. In the first five minutes, there is a very small and rapid increase in the absolute values of the potential. This initial increase is immediately followed by a decrease in the absolute value of the potential during the next 20 minutes. This behavior can be explained by the nucleation and growth of Sb from the oxaline [10, 40]:

Nucleation Phase:

During the initial stages of electrodeposition, a high initial overpotential is required to overcome the activation energy barrier for the nucleation of Sb. As nucleation sites start forming on the electrode surface, these sites act as initial anchors for the deposited material. The potential initially increases as the system works to create these nucleation sites.

Growth Phase:

- Once nucleation sites are established, the surface area available for deposition increases. This means that more Sb can deposit simultaneously, which can lower the local current density at each nucleation site. With the increase in the number of nucleation sites and the surface area, the overpotential required for further deposition decreases. This results in a decline in the absolute value of the potential.

- The system transitions from a high-energy nucleation phase to a lower-energy growth phase. This transition is characterized by a decline in potential as the system stabilizes and the rate of Sb deposition becomes more uniform.

After the nucleation and growth period, the potential stabilizes around -0.91 V. The stabilization of the potential suggests that a steady-state deposition process is achieved. At this point, the rate of Sb deposition on the electrode surface balances with the electrochemical reactions occurring, indicating a consistent and controlled deposition environment.

The fluctuations in potential during the experiment are similar to the fluctuations in current that were observed during the potentiostatic experiments. They may be due to slight variations in the local environment at the electrode surface, such as changes in concentration or slight disturbances in the electrochemical cell, in addition to the sample taking. However, the galvanostatic electrodeposition demonstrates an overall stability of the potential.

4.4.2.2. Galvanostatic electrodeposition at -0.62 mA/cm²

The second galvanostatic electrodeposition experiment of oxaline with 10 mM Sb was conducted at a constant current of -0.62 mA/cm^2 and the potential profile over time is shown in Figure 36.

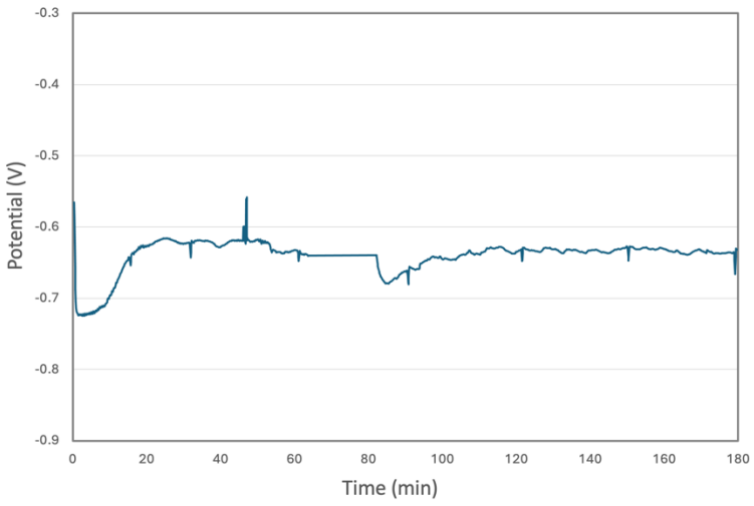

Figure 36: Galvanostatic Electrodeposition of Oxaline with 10 mM Sb at a current of -0.62 mA/cm².

Similarly to the experiment conducted at -1.27 mA/cm^2, there is an initial short and rapid increase in the absolute value of the potential can be verified followed by a decrease before stabilizing to the steady-state period.

The evolution of the curve is similar with the same three phases (nucleation, growth, and steady-state phase), a detailed explanation on the nucleation and growth phases can be found in Chapter 4, Section 4.4.2.1: 'Galvanostatic electrodeposition at -1.27 mA/cm²'. Although these similarities there are some differences and additional observations:

The overall potential values are less negative at -0.62 mA/cm^2 compared to the -1.27 mA/cm^2 experiment. This indicates a lower overpotential required for the deposition process at the reduced current densities, which is consistent with the behavior expected under galvanostatic conditions. Lower overpotential at a reduced current is typical because the driving force for the electrochemical reaction is lower when the applied current is reduced. At higher currents, the electrode surface must sustain higher rates of electron transfer, leading to increased energy demand and thus a more negative potential. Conversely, at lower currents, the electrode reaction kinetics are more favorable, requiring less energy to maintain the same reaction rate, resulting in less negative potentials.

Furthermore, this observation suggests that the deposition kinetics of antimony at -0.62 mA/cm² are more efficient compared to the higher current of -1.27 mA/cm^2, which was also confirmed by the LSV. The reduced overpotential could indicate better utilization of the electrochemical energy for the deposition process, potentially leading to a more uniform and controlled film growth. This insight is crucial for optimizing electrodeposition parameters, as operating at a lower current may enhance the quality of the deposited film while maintaining efficient deposition rates.

Another difference is the more pronounced fluctuations and occasional spikes in potential that can be observed throughout the deposition period at -0.62 mA/cm^2. These variations are notably more significant compared to other experiments conducted at different current densities. The pronounced fluctuations and spikes in potential may be attributed, in addition to the previously discussed causes, to several factors, with the formation and detachment of gas bubbles being two key contributors.

These gas bubbles can temporarily adhere to the electrode surface, creating a barrier that impedes the normal flow of current and alters the potential. When these bubbles eventually detach from the surface, they cause sudden changes or spikes in potential as the current flow momentarily stabilizes. This process of formation and detachment of gas bubbles is significantly more prominent in the experiment conducted at -0.62 mA/cm^2 compared to other experiments. This phenomenon is illustrated in Figure 37, where the gas bubbles can be observed in the DES solution on and near the electrode surface.

Figure 37: Formation and detachment of gas bubbles during (Galvanostatic) electrodeposition experiment.

Refer to the explanation provided for the -1.27 mA/cm^2 experiment (Section 4.4.2.1) for a detailed understanding of the nucleation and growth phases.

4.4.2.3. Galvanostatic electrodeposition at -0.18 mA/cm²

The third galvanostatic electrodeposition experiment of oxaline with 10 mM Sb was conducted at a constant current of -0.18 mA/cm², as shown in Figure 38. Similarly to the previous experiments conducted at -1.27 mA/cm² and -0.62 mA/cm², an initial short and rapid increase in the absolute value of the potential can be seen followed by a decrease before stabilizing to the steady-state period. However, due to data recording limitations, the data for the initial part (rapid increase and decrease) was lost.

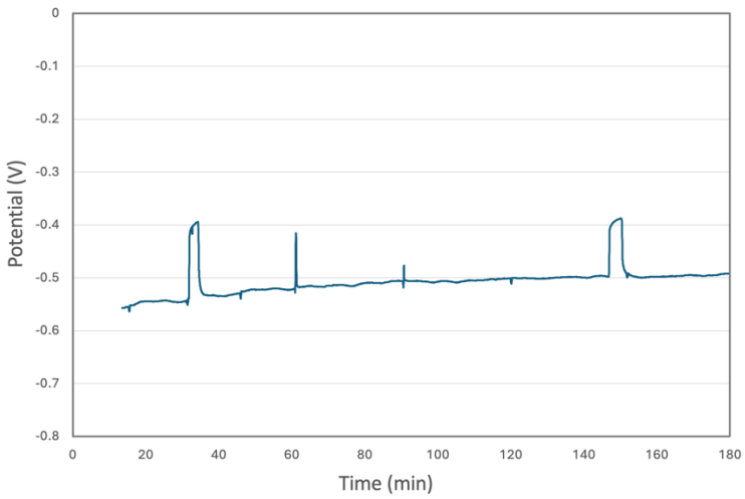

Figure 38: Galvanostatic Electrodeposition of Oxaline with 10 mM Sb at a current of -0.18 mA/cm².

Although the initial part was lost and cannot be analyzed, the steady-state phase was recorded. Overall, the potential values are less negative at -0.18 mA/cm^2 compared to the -1.27 mA/cm^2 and -0.62 mA/cm^2 experiments. As explained previously, this indicates a lower overpotential required for the deposition process at the reduced current, which is consistent with the behavior expected under galvanostatic conditions.

4.4.2.4. Galvanostatic electrodeposition Summary Graph

The provided graph shown in Figure 39 shows the LSV represented by the blue curve, alongside three steady-state electrode potential values (red dots) obtained from galvanostatic electrodeposition over a duration of 3 hours at different current densities.

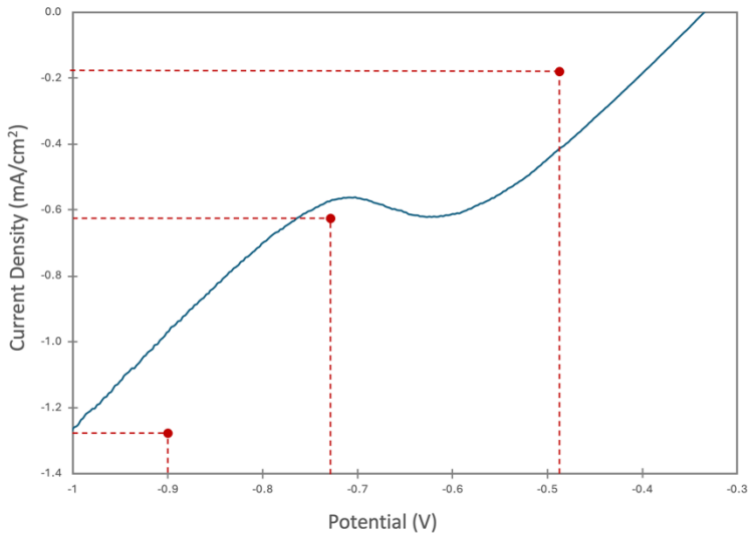

Figure 39: Steady-state values (red dots) of the electrode potential obtained by galvanostatic electrodeposition, together with the LSV at 80 °C represented by the blue curve.

The agreement between the steady-state electrode potential values (red dots) and the LSV (blue curve) is quite good, indicating consistency in the observed trends. Before and during the peak, more cathodic potentials are reached, reflecting the high reactivity and electron transfer rates under these conditions. However, beyond the peak (reduction wave), less cathodic potentials are registered, likely due to the onset of hydrogen evolution reaction (HER), which becomes significantly more prominent during long-term experiments. This transition suggests that while the initial electrochemical reduction processes dominate near the peak, the prolonged application of current density enhances the diffusion limitations and HER activity, leading to a shift in the observed steady-state potentials.

4.4.3. Electrodeposition Analysis

4.4.3.1. Visual Examination of Electrodes

The initial state of the working electrode is shown in Figure 40. The electrode was cleaned and sanded up to grid 4000 and dried to ensure a smooth and clean surface, optimal for the following electrodeposition experiments.

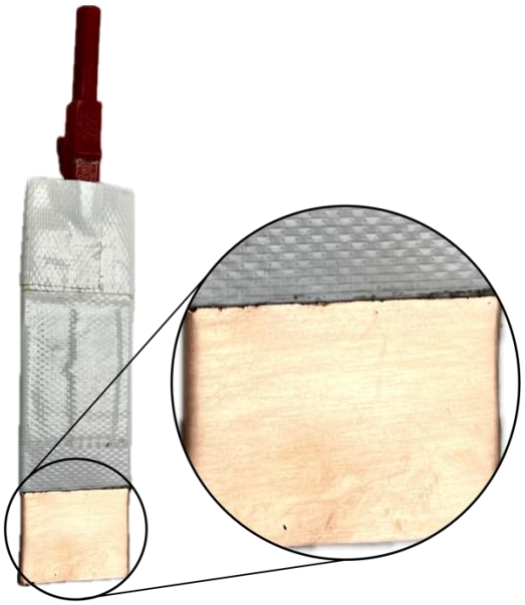

Figure 40: Working electrode before electrodeposition experiment.

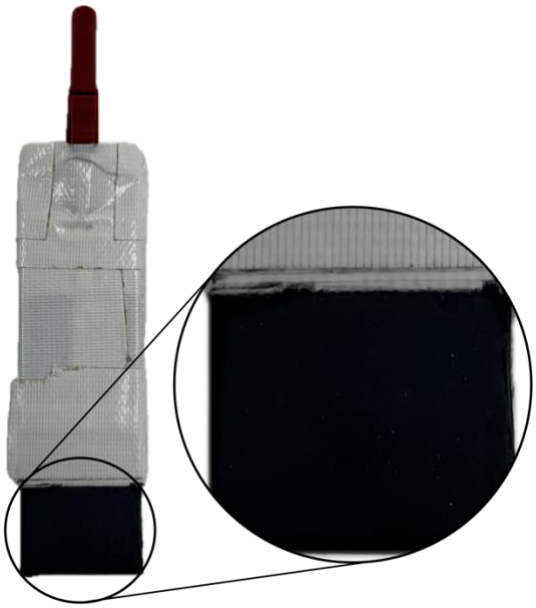

Figure 41: Working electrode after potentiostatic electrodeposition at -600 mV.

Following the potentiostatic electrodeposition at -600 mV, a visual inspection of the electrode shown in Figure 41 shows a significant change in the surface appearance. The electrode surface is coated with a darker layer, indicating the successful deposition of antimony.

Upon conducting various electrodeposition experiments under different conditions (potentiostatic at -400 mV and -800 mV, and galvanostatic at -0.18 , -0.62, and -1.27 mA/cm^2), it was observed that the visual appearance of the deposited layers was indistinguishable for these conditions. Each condition resulted in a consistent and uniform deposition of antimony on the electrode surface, similar to the appearance shown in Figure 41.

The potentiostatic electrodeposition experiment (at -600 mV) of the solution with 10 % v/v 0.3M HCl, is depicted in Figure 42. The resulted electrode shows a significantly different surface morphology. The addition of HCl resulted in a more textured, more granular and a thicker deposit. This rough texture suggests an increased nucleation rate during the deposition process, resulting in a higher density of deposited antimony particles.

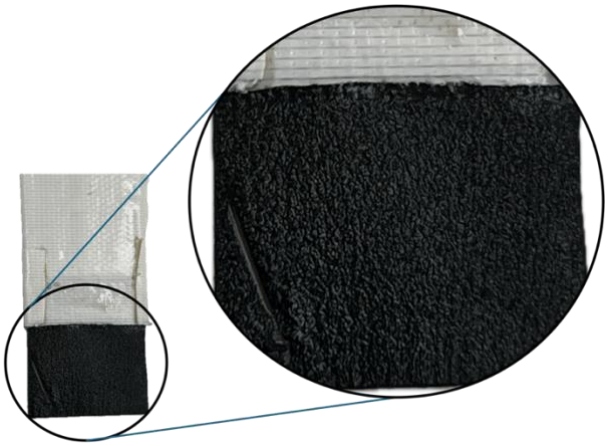

Figure 42: Working electrode after potentiostatic electrodeposition at -600 mV with the addition of HCl.

The electrodeposits do not show any visible defects such as cracks or peeling; however, during the experiment, small pieces of the deposition came loose and were visible in the solution, as can be seen in Figure 43. This occurred because of the increased granular nature of the deposited layer, which have reduced the adhesion strength between the antimony layer and the electrode substrate. The rough and granular texture creates points of weakness where the deposition is more likely to detach under the influence of the electrolyte solution or mechanical agitation.

Figure 43: Detached antimony deposition in the solution during the potentiostatic electrodeposition at -600 mV with the addition of HCl.

4.4.3.2. AAS and Weight analysis

During the electrodeposition experiments without HCl, it was not possible to detect a significant weight difference in the electrodes before and after the deposition. This indicates that the antimony layer deposited was too thin to measure accurately with the available equipment.

In the experiment with HCl added to the solution, the deposition was significantly thicker, as discussed previously. This increased thickness made it possible to measure the weight gain due to the antimony deposition. The mass of the electrode before the experiment was 33.9358 g, and after the deposition, it increased to 33.9732 g, resulting in a gain of 0.0374 g. This indicates the successful deposition of a measurable amount of antimony.

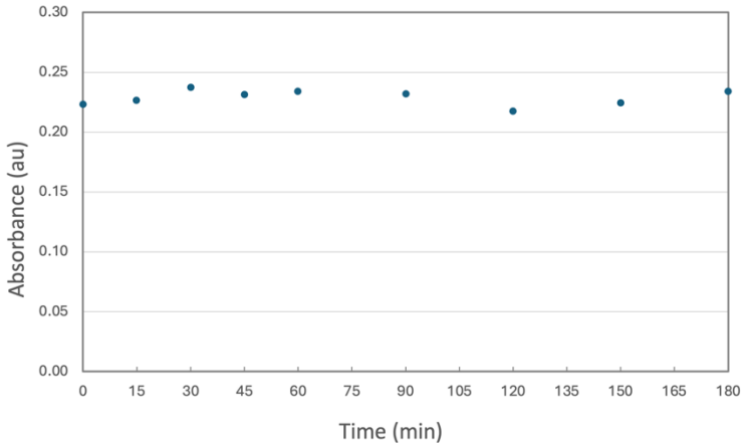

Figure 44: Concentration profile of antimony during the electrodeposition experiment with HCl.

Despite these observations, it was not possible to measure a decline in the antimony concentration in the solution using AAS, as can be seen in Figure 44. Neither the concentration near the electrode nor the overall concentration in the solution showed a detectable change due to the deposited antimony. Even with the thicker antimony layer observed in the HCl experiment, no significant concentration change was detected in the solution. This suggests that the amount of antimony deposited might be too small relative to the total concentration of the solution to cause a noticeable change in concentration, or that the deposition efficiency does not significantly deplete the antimony ions from the bulk solution.

4.4.3.3. Solution changes

The solution undergoes a noticeable change in color as a result of the deposition experiment, as depicted in Figure 45. Initially, the solution appears milky white, and after the experiment, it shows a distinct yellowing.

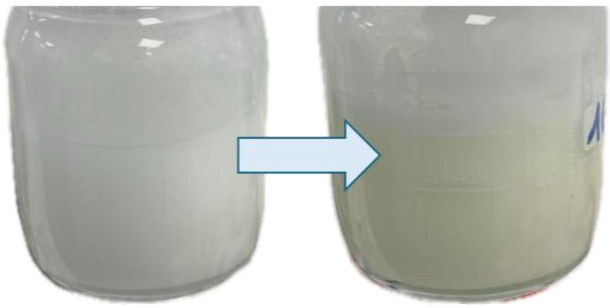

Figure 45: Solution changes due to the deposition experiment (yellowing).

During the experiment, the viscosity of the solution increases even though the temperature is maintained constantly at 80 °C. After the experiment, the solution appears more yellow than before, and upon cooling down to room temperature, it solidifies. This indicates that while the melting point of the eutectic solvent was initially lower than room temperature, it increased during the experiment, resulting in the solution becoming solid at room temperature.

Before electrodeposition, the addition of HCl significantly lowered the viscosity of the solution and changed its appearance from opaque to completely transparent. After the deposition experiment, as shown in Figure 46, the solution remains transparent but undergoes noticeable yellowing.

Figure 46: Solution changes due to the addition of HCl and

The viscosity of the solution before and after the experiment remains the same, and in contrast to the experiment without HCl, there is no solidification upon cooling down to room temperature.

Chapter 6

Conclusions

This study investigates the use of deep eutectic solvents, specifically oxaline, for the recovery of antimony by means of electrodeposition. The research is motivated by the critical importance of antimony in various industrial applications and the need for sustainable recovery methods due to environmental and safety concerns associated with traditional solvents like hydrochloric acid.

The eutectic solvent oxaline, consisting of choline chloride and oxalic acid in a 1:1 molar ratio, was prepared and characterized. The choice of this type of solvent is based among other on its green chemistry attributes, including low toxicity, high availability and reduced volatility. The dissolution experiments revealed that antimony(III)chloride ($SbCl_3$) is more soluble in oxaline compared to antimony(III)oxide (Sb_2O_3), making it more suitable for subsequent electrochemical experiments.

Cyclic voltammetry and linear sweep voltammetry were utilized to analyze the electrochemical behavior of oxaline and antimony-containing solutions. These techniques provided valuable insights into the redox potentials and kinetics of the system. The voltammograms indicated that the electrodeposition of antimony occurs at specific potential ranges, which were further explored in electrodeposition experiments.

The potentiostatic electrodeposition experiments, conducted at various potentials (-400 mV, -600 mV, -800 mV), demonstrated successful antimony deposition. The optimal results were obtained at -600 mV, corresponding to the reduction peak potential identified in LSV. The addition of HCl to the solution lowered the viscosity and improved deposition rates, resulting in thicker antimony layers. However, it was observed that some of the deposited antimony layers detached from the electrode surface. Galvanostatic electrodeposition, performed at different current densities (-0.18 mA/cm^2, -0.62 mA/cm^2, -1.27 mA/cm^2), confirmed the findings from potentiostatic deposition, showing effective antimony recovery under controlled conditions.

Despite successful deposition, the overall change in antimony concentration in the solution and the increase in antimony deposition mass were minimal, indicating that process efficiency

needs improvement for practical applications. Additionally, the solution showed a further increase in viscosity after electrodeposition, which lowered mass transport even more. The physical appearance of the solution also changed from a white (milky) color to a more yellow color.

This study has shown that deep eutectic solvents like oxaline can provide a sustainable alternative for antimony recovery. The approach aligns with the principles of green chemistry and contributes to the sustainable development goals (SDGs).

Future research on this topic is needed and could focus further on reducing the viscosity to improve mass transport. Additionally, investigating the reusability of oxaline after electrodeposition for antimony recovery would be beneficial.

In conclusion, despite the mass transport limitations due to high viscosity, this research has demonstrated the potential of using DES for the recovery of critical raw materials like antimony, offering a greener and safer alternative to conventional methods.

Part II

Budget

Chapter 7

Budget Break Down

6.1. Budgeting Overview

Calculating the budget or cost of a project is a crucial step. In this chapter, the cost of the project for the master thesis is estimated by categorizing the costs into five distinct sections:

- Labor Cost
- Depreciation Cost of Instruments and Equipment
- Licenses
- Consumables and Materials
- Waste Management

Once a detailed breakdown of these costs is available, the total cost of the project will be calculated in the subsequent chapter.

This total cost will then be subjected to General Expenses, which typically account for 13 % of the total cost. These expenses encompass overhead costs such as utilities like electricity, water, heating, etc.

Finally, the cost, inclusive of the general expenses, will be subjected to a Value Added Tax (VAT) of 21 %. This tax is levied on the value added to the product or service at each stage of production or distribution.

6.2. Price Lists

6.2.1. Labor Cost

The Labor Cost (LC) represents the expenses associated with the human resources involved in the project. This thesis was completed by a chemical engineering student, with the academic

and experimental work managed and contributed to by a PhD Researcher acting as Co-tutor and a University Professor as the main Tutor.

The total labor cost is determined by multiplying the hourly rate by the number of hours each individual contributed to the project. The hourly rates are considered to be € 15 for the student, € 30 for the co-tutor, and € 40 for the tutor. The results are presented in Table 8.

Table 8: Budget - Labor Cost.

Labor Cost					
Ref	**Unit**	**Description**	**Price per hour (€/h)**	**Amount**	**Subtotal (€)**
LC1	h	Student - Chemical Engineer	15.00	300	4,500.00
LC2	h	Co-tutor - PhD Researcher	30.00	100	3,000.00
LC3	h	Tutor - University Professor	40.00	50	2,000.00
				TOTAL	**9,500.00**

The expenditure associated with the labor required to complete the project amounts to **NINE THOUSAND FIVE HUNDRED EUROS.**

6.2.2. Instrument Depreciation and License Cost

In the subsequent section of the budget estimation, the depreciation cost of the instruments and equipment utilized during the project is accounted for. The lifespan of the equipment is estimated to be approximately 10 years, with the assumption that a year comprises roughly 1600 working hours. The portion of the budget allocated to depreciation is calculated based on the equipment's temporary usage period of about 3 months.

The price of the equipment includes the license for its associated software. The costs for any additional software, not included with the equipment, are calculated separately and detailed in Table 9.

Table 9: Budget - Depreciation & License Cost.

Depreciation & License Cost							
Ref	**Unit**	**Description**	**Price (€)**	**Service Life (Y)**	**Price per hour (€/h)**	**Amount**	**Subtotal (€)**
D1	h	AUTOLAB	16,730.00	10	1.046	75	78.42
D2	h	Computer	1,200.00	10	0.075	75	5.63

D3	h	Office License	99.00	1	0.062	300	18.56
D4	h	Precision Balance	2,447.00	10	0.153	2	0.31
D5	h	Magnetic Stirrer Hotplate	800.00	10	0.050	150	7.50
D6	h	AAS - Instrument	20,000.00	10	1.250	15	18.75
						TOTAL	**129.17**

The costs related to the depreciation of the instruments and equipment, along with the software license cost, are calculated to be **ONE HUNDRED TWENTY-NINE EUROS AND SEVENTEEN CENTS.**

6.2.3. Consumables and Material

The cost of the consumables and laboratory materials used is a crucial component in the total cost calculation of the project. This cost is calculated by multiplying the unit price of the consumables and laboratory materials by the quantity used during the project. For some bulk materials, the unit price is calculated by dividing the total price by the number of units in the bulk. The unit prices, as well as the calculated costs for the project, are shown in Table 10.

Table 10: Budget - Consumables & Materials Cost.

Consumables & Materials Cost					
Ref	**Unit**	**Description**	**Price per unit (€/ud.)**	**Amount**	**Subtotal (€)**
M1	Ud.	Digital Multimeter	44.93	1	44.93
M2	Ud.	Adjustable micropipette 100-1000 µL	287.00	1	287.00
M3	Ud.	Micropipette tips	0.12	20	2.46
M4	Ud.	Pyrex 50 mL volumetric flask (SLW3151/12)	15.72	10	157.20
M5	Ud.	Pyrex 100 mL volumetric flask (SLW3151/14)	19.44	2	38.88

M6	Ud.	Pyrex 250 mL volumetric flask (SLW3151/18)	27.05	2	54.10
M7	Ud.	Pyrex 1000 mL volumetric flask (SLW3151/22)	48.30	1	48.30
M8	Ud.	Duran 100 mL laboratory bottles	18.70	5	93.50
M9	Ud.	Disposable Pasteur pipettes	0.28	3	0.83
M10	Ud.	100 mL beaker	4.96	1	4.96
M11	Ud.	Universal stand	160.00	1	160.00
M12	Ud.	Adjustable angle universal clamp	26.00	3	78.00
M13	Ud.	Fine sandpaper (grain 4000)	1.21	2	2.42
M14	Ud.	Coarse sandpaper (grain 5000)	0.65	2	1.30
M15	Ud.	Laboratory cables with connections	4.10	2	8.20
M16	Ud.	Copper electrode	8.97	1	8.97
M17	Ud.	Titanium electrode	18.40	1	18.40
M18	Ud.	Ag/AgCl electrode	176.00	2	352.00
M19	Ud.	Rotating disk-ring electrode, platinum disk	242.00	1	242.00
M20	Ud.	Conventional three-electrode cell	90.76	1	90.76
M21	Ud.	Box of nitrile gloves	3.57	1	3.57
M22	Ud.	Stirring magnet	4.50	3	13.50
				TOTAL	**1,711.28**

The cost of the used Consumables & Materials in the project comes up to a **THOUSAND SEVEN HUNDRED ELEVEN EUROS AND TWENTY-EIGHT CENTS.**

6.2.4. Reagents and Compounds

Next in the budget estimation is the cost of the reagents and compounds, presented in Table 11. This includes all the chemicals, solutions, and compounds required for the project. The cost of each reagent is calculated based on its unit price and the quantity used in the project.

The unit price is determined by dividing the price of the bulk container by the quantity in the bulk order. The cost for each reagent (subtotal) is then calculated by multiplying this unit price with the amount used. The total cost of reagents and compounds is the sum of the subtotals of all the reagents used in the project.

I this estimation it is assumes that all reagents and compounds, including distilled water, are purchased specifically for the project and are not already available in the inventory.

Table 11: Budget - Reagents & Compounds Cost.

Reagents and Compounds Cost					
Ref	**Unit**	**Description**	**Price per unit (€)**	**Amount**	**Subtotal (€)**
R1	g	Sigma - Aldrich Oxalic Acid (194131-1KG)	0.148	790.34	116.97
R2	g	Sigma - Aldrich Choline chloride (C1879-1KG)	0.128	1225.98	156.93
R3	g	Sigma - Aldrich Antimony(III)chloride (8146560250)	0.584	3.4411	2.01
R4	g	Sigma - Aldrich Antimony(III)oxide (230898-100G)	0.484	0.6067	0.29
R5	L	Distilled Water	0.38	30	11.40
R6	L	HCl 12 M (37 % Panreac)	24.8	1	24.80
				TOTAL	**312.40**

The total cost for this part of the budget calculation, which includes the cost of reagents and compounds, has been accurately estimated to be **THREE HUNDRED TWELVE EUROS AND FORTY CENTS.**

6.2.5. Waste Management

According to the Environmental Unit of UPV, waste management costs are calculated based on the weight of the waste transported, with an additional cost of €200 per transfer and a transport capacity of 4000 kilos per trip. This results in a cost of €0.05 per kilo of waste, which is shown in Table 12.

Table 12: Budget - Waste Management Cost.

Waste Management Cost					
Ref	**Unit**	**Description**	**Price per unit (€)**	**Amount**	**Subtotal (€)**
W1	kg	Group 04: Inorganic acids and acid solutions with metals	0.35	3	1.05
W2	kg	Waste shipment	0.05	3	0.15
				TOTAL	**1.20**

The cost associated with the waste is **ONE EURO AND TWENTY CENTS.**

Chapter 8

Total Budget

In this chapter, the sum of the previous cost breakdown is calculated and shown in Table 13. After an overhead is included as “general expenses” of 13 % of the previous total cost. After which a tax of 21 % VAT is calculated giving the Total budget / Cost of the master thesis project.

Table 13: Total Budget.

Description	Subtotal (€)
Labor	9,500.00
Instrument Depreciation and Licenses	129.17
Consumables & Materials	1,711.28
Reagents and Compounds	312.40
Waste Management	1.20
TOTAL BEFORE GENERAL EXPENSES AND TAXES	11,654.05
GENERAL EXPENSES 13%	1,515.03
TOTAL BEFORE TAXES	13,169.08
VAT 21%	2,765.50
TOTAL AFTER TAXES	**15,934.58**

The final figure, inclusive of the VAT, comes to € 15,934.58 or **FIFTEENTHOUSAND NINEHUNDRED THIRTYFOUR EUROS AND FIFTYEIGHT CENTS.** This represents the total budget or cost of the master thesis project.

Bibliography

[1] "Antimony Statistics and Information | U.S. Geological Survey." https://www.usgs.gov/centers/national-minerals-information-center/antimony-statistics-and-information#:~:text=Estimates%20of%20the%20abundance%20of,lead%2C%20copper%2C%20and%20silver.

[2] Federal Ministry of Finance, "World Mining Data - World Mining Data," Austrian Federal Ministry of Finance (BMF), ISBN 978-3-901074-57-8, Apr. 2024. Accessed: Mar. 01, 2024. [Online]. Available: https://world-mining-data.info/wmd/downloads/PDF/WMD%202024.pdf

[3] European Commission, Directorate-General for Internal Market, and Industry, Entrepreneurship and SMEs, "Study on the Critical Raw Materials for the EU 2023 : Final report," Publications Office of the European Union, ET-07-23-116-EN-N, 2023. Accessed: Feb. 14, 2024. [Online]. Available: https://data.europa.eu/doi/10.2873/725585

[4] D. C. Paz-Gómez, S. M. Pérez-Moreno, I. Ruiz-Oria, G. Ríos, and J. P. Bolívar, "Characterization of Two Sludges from a Pyrometallurgical Copper Smelting Complex for Designing a Se and Pb Recovery Proposal," *Waste and Biomass Valorization*, vol. 12, no. 5, pp. 2739–2755, Aug. 2020, doi: 10.1007/s12649-020-01197-w.

[5] T. E. Achkar, H. Greige-Gerges, and S. Fourmentin, "Basics and properties of deep eutectic solvents: a review," *Environmental Chemistry Letters*, vol. 19, no. 4, pp. 3397–3408, Apr. 2021, doi: 10.1007/s10311-021-01225-8.

[6] K. El-Deen and K. Shimizu, "Deep eutectic solvents as promising green solvents in dispersive Liquid–Liquid microextraction based on solidification of floating organic droplet: recent applications, challenges and future perspectives," *Molecules/Molecules Online/Molecules Annual*, vol. 26, no. 23, p. 7406, Dec. 2021, doi: 10.3390/molecules26237406.

[7] M. Da Costa Lopes, "Biomass delignification with green solvents towards lignin valorisation: ionic liquids vs deep eutectic solvents," *Acta Innovations*, no. 40, pp. 64–78, Sep. 2021, doi: 10.32933/actainnovations.40.5.

[8] E. L. Smith, A. P. Abbott, and K. S. Ryder, "Deep Eutectic Solvents (DESS) and their applications," *Chemical Reviews*, vol. 114, no. 21, pp. 11060–11082, Oct. 2014, doi: 10.1021/cr300162p.

[9] N. Elgrishi, K. J. Rountree, B. D. McCarthy, E. S. Rountree, T. T. Eisenhart, and J. L. Dempsey, "A practical Beginner's guide to cyclic voltammetry," *Journal of Chemical*

Education, vol. 95, no. 2, pp. 197–206, Nov. 2017, doi: 10.1021/acs.jchemed.7b00361.

[10] G. Inzelt, "Kinetics of electrochemical reactions," in *Springer eBooks*, 2009, pp. 33–53. doi: 10.1007/978-3-642-02915-8_3.

[11] T. Wang *et al.*, "Palladium alloys used as electrocatalysts for the oxygen reduction reaction," *Energy & Environmental Science*, vol. 14, no. 5, pp. 2639–2669, Jan. 2021, doi: 10.1039/d0ee03915b.

[12] Libretexts, "6.2.3.3: The Arrhenius Law - Activation Energies," *Chemistry LibreTexts*, Feb. 13, 2023. https://chem.libretexts.org/Bookshelves/Physical_and_Theoretical_Chemistry_Textbook_Maps/Supplemental_Modules_%28Physical_and_Theoretical_Chemistry%29/Kinetics/06%3A_Modeling_Reaction_Kinetics/6.02%3A_Temperature_Dependence_of_Reaction_Rates/6.2.03%3A_The_Arrhenius_Law/6.2.3.03%3A_The_Arrhenius_Law-_Activation_Energies

[13] European Union's Horizon 2020 research and innovation programme, "CRMS 2023 - ANTIMONY," Feb. 2024. Accessed: Feb. 27, 2024. [Online]. Available: https://scrreen.eu/crms-2023/

[14] D. Dupont, S. Arnout, P. T. Jones, and K. Binnemans, "Antimony Recovery from End-of-Life Products and Industrial Process Residues: A Critical Review," *Journal of Sustainable Metallurgy*, vol. 2, no. 1, pp. 79–103, Feb. 2016, doi: 10.1007/s40831-016-0043-y.

[15] David, "Oxidizing roast; stibnite the antimony mineral," *Metallurgist & Mineral Processing Engineer*, Apr. 10, 2017. https://www.911metallurgist.com/behavior-stibnite-oxidizing-roast/ (accessed Jun. 10, 2024).

[16] R. Padilla, A. Aracena, and M. C. Ruiz, "Kinetics of stibnite (Sb2S3) oxidation at roasting temperatures," *Journal of Mining and Metallurgy. Section B, Metallurgy/Journal of Mining and Metallurgy. Section B, Metallurgy*, vol. 50, no. 2, pp. 127–132, Jan. 2014, doi: 10.2298/jmmb130131012p.

[17] R. Padilla, L. C. Chambi, and M. C. Ruiz, "Antimony production by carbothermic reduction of stibnite in the presence of lime," *Journal of Mining and Metallurgy. Section B, Metallurgy/Journal of Mining and Metallurgy. Section B, Metallurgy*, vol. 50, no. 1, pp. 5–13, Jan. 2014, doi: 10.2298/jmmb130604003p.

[18] Libretexts, Department of Education Open Textbook Pilot Project, UC Davis Office of the Provost, UC Davis Library, and California State University, "25.3: Linear sweep voltammetry," *Chemistry LibreTexts*, Mar. 13, 2023. https://chem.libretexts.org/Bookshelves/Analytical_Chemistry/Instrumental_Analy

sis_%28LibreTexts%29/25%3A_Voltammetry/25.03%3A_Hydrodynamic_Voltammetry (accessed Jun. 05, 2024).

[19] "MIT OpenCourseWare," *MIT OpenCourseWare*, May 2014. https://ocw.mit.edu/courses/10-626-electrochemical-energy-systems-spring-2014/pages/lecture-notes/ (accessed May 24, 2024).

[20] J. Newman and N. P. Balsara, *Electrochemical systems*. John Wiley & Sons, 2021.

[21] "Basics of Green Chemistry | US EPA," *US EPA*, May 02, 2024. https://www.epa.gov/greenchemistry/basics-green-chemistry (accessed Jun. 15, 2024).

[22] "12 Principles of Green Chemistry - American Chemical Society," *American Chemical Society*. https://www.acs.org/greenchemistry/principles/12-principles-of-green-chemistry.html (accessed Jun. 15, 2024).

[23] M. G. Montalbán and G. Víllora, "Supercritical Fluids: Properties and Applications," in *IntechOpen eBooks*, 2022. doi: 10.5772/intechopen.105485.

[24] F. U. Shah, R. An, and N. Muhammad, "Editorial: Properties and Applications of Ionic Liquids in Energy and Environmental Science," *Frontiers in Chemistry*, vol. 8, Dec. 2020, doi: 10.3389/fchem.2020.627213.

[25] "Three-Electrode Setups," *Pine Research Instrumentation Store*, May 23, 2019. https://pineresearch.com/shop/kb/applications/rde-and-rrde/three-electrode-setups/ (accessed Jun. 17, 2024).

[26] University of Cambridge, "Linear Sweep and Cyclic Voltametry: The Principles," *Department of Chemical Engineering and Biotechnology*. https://www.ceb.cam.ac.uk/research/groups/rg-eme/Edu/linear-sweep-and-cyclic-voltametry-the-principles (accessed Jun. 17, 2024).

[27] Topics, "Atomic Absorption Spectroscopy (AAS) | Study Chemistry," *Medium*, Nov. 17, 2022. Accessed: May 22, 2024. [Online]. Available: https://medium.com/study-chemistry/atomic-absorption-spectroscopy-aas-f372e4622923

[28] "Atomic Absorption Spectroscopy, How Does AAS Work, AAS FAQs | Agilent." https://www.agilent.com/en/support/atomic-spectroscopy/atomic-absorption/flame-atomic-absorption-instruments/how-does-aas-work-aas-faqs (accessed May 15, 2024).

[29] H. Hashimoto, T. Nishimura, and Y. Umetsu, "Hydrolysis of Antimony(III)-Hydrochloric Acid Solution at 25°C," *Materials Transactions*, vol. 44, no. 8, pp. 1624–1629, Jan. 2003, doi: 10.2320/matertrans.44.1624.

[30] "Diffusion and Kinetic Controlled Electrochemical Reactions - Wolfram Demonstrations Project."

https://demonstrations.wolfram.com/DiffusionAndKineticControlledElectrochemicalReactions/ (accessed Jun. 20, 2024).

[31] A. V. Kosov, O. V. Grishenkova, V. A. Isaev, and Y. Zaikov, “Simulation of Diffusion-Controlled Growth of Interdependent Nuclei under Potentiostatic Conditions,” *Materials*, vol. 15, no. 10, p. 3603, May 2022, doi: 10.3390/ma15103603.

[32] H. Hashimoto, T. Nishimura, and Y. Umetsu, “Hydrolysis of Antimony(III)-Hydrochloric Acid Solution at 25°C,” *Materials Transactions*, vol. 44, no. 8, pp. 1624–1629, Jan. 2003, doi: 10.2320/matertrans.44.1624.

[33] “Oxalic Acid 98 144-62-7.” https://www.sigmaaldrich.com/ES/en/product/aldrich/194131 (accessed May 13, 2024).

[34] “Choline chloride, powder or crystals, 67-48-1, Sigma-Aldrich.” https://www.sigmaaldrich.com/ES/en/product/sigma/c1879 (accessed Jun. 13, 2024).

[35] “Antimony(III) Chloride for Synthesis 10025-91-9.” https://www.sigmaaldrich.com/ES/en/product/mm/814656 (accessed Jun. 13, 2024).

[36] “Antimony(III) oxide powder, 5um, ReagentPlus , 99 1309-64-4.” https://www.sigmaaldrich.com/ES/en/product/aldrich/230898 (accessed Jun. 13, 2024).

[37] “Ácido clorhídrico 37% (máx. 0,0000005% hg) (Reag. USP) para análisis, ACS, ISO.” https://www.itwreagents.com/iberia/es/product/acido-clorhidrico-37-reag-usp-para-analisis-acs-iso/131020 (accessed May 26, 2024).

[38] “Digital multimeter, suitable for measuring AC/DC current, AC/DC voltage, resistance, battery voltage, temperature, including test leads,” *Velleman DVM892N: Digital Multimeter, Suitable for Measuring AC/DC Current, AC/DC Voltage, Resistance, Battery Voltage, Temperature, Including Test Leads – Velleman – Wholesaler and Developer of Electronics*. https://www.velleman.eu/products/view/?id=435328&lang=en (accessed May 25, 2024).

[39] “Fisherbrand™ Micropipetas de volumen ajustable Elite™ -.” https://www.fishersci.es/shop/products/fisherbrand-elite-adjustable-volume-pipetters-13/p-4249384#?keyword= (accessed May 23, 2024).

[40] R. Hamdi *et al.*, “Electrodeposition Study of Silver: Nucleation process and theoretical analysis,” *Journal of Electronic Materials*, vol. 50, no. 10, pp. 5507–5513, Jul. 2021, doi: 10.1007/s11664-021-09055-8.

[41] Libretexts, “7: Electrical conductivity of aqueous solutions (Experiment),” *Chemistry LibreTexts*, Oct. 15, 2022. https://chem.libretexts.org/Ancillary_Materials/Laboratory_Experiments/Wet_Lab_Experiments/General_Chemistry_Labs/Online_Chemistry_Lab_Manual/Chem_9_Experiments/07%3A_Electrical_Conductivity_of_Aqueous_Solutions_%28Experiment%29 (accessed Jun. 17, 2024).

[42] Libretexts, “3.3A: diffusion,” *Medicine LibreTexts*, Jan. 17, 2023. https://med.libretexts.org/Bookshelves/Anatomy_and_Physiology/Anatomy_and_Physiology_(Boundless)/3%3A_Organization_at_the_Cellular_Level/3.3%3A_Transport_Across_Membranes/3.3A%3A_Diffusion (accessed Jun. 18, 2024).

Appendices

Solution 1	Oxalic Acid		Choline Chloride	
	mass (g)	moles	mass (g)	moles
1	4.4931	0.0499067	6.9792	0.04998711
2	10.217	0.11348439	15.4559	0.11069976
3	15.1659	0.16845385	25.4656	0.18239221
4	1.6724	0.01857603	1.0399	0.00744807
Total	31.5484	0.35042097	48.9406	0.35052715
Added mass (Sb2O3) (g)		0.0909		

Solution 2	Oxalic Acid		Choline Chloride	
	mass (g)	moles	mass (g)	moles
1	4.6829	0.0520	7.0532	0.0505
2	15.1985	0.1688	23.6368	0.1693
3	11.6455	0.1294	18.2071	0.1304
Total	31.5269	0.3502	48.8971	0.3502
Added mass (Sb2O3) (g)		0.0907		

Solution 3 (20 mM Sb)	Oxalic Acid		Choline Chloride	
	mass (g)	moles	mass (g)	moles
1	5.7586	0.0640	8.9217	0.0639
2	10.9291	0.1214	15.5779	0.1116
3	15.1744	0.1685	25.5987	0.1833
4	4.7355	0.0526	6.6637	0.0477
Total	36.5976	**0.4065**	56.7620	**0.4065**
Added mass (Sb2O3) (g)		0.2431		

Solution 4	Oxalic Acid		Choline Chloride	
	mass (g)	moles	mass (g)	moles
1	6.2847	0.0698	9.7621	0.0699
2	11.0426	0.1227	15.9682	0.1144
3	15.3887	0.1709	25.5022	0.1827
4	3.8836	0.0431	5.5306	0.0396
Total	36.5996	**0.4065**	56.7631	**0.4066**
Added mass (SbCl3) (g)		0.1943		

Solution 5	Oxalic Acid		Choline Chloride	
	mass (g)	moles	mass (g)	moles
1	5.8369	0.0648	9.0469	5.8369
2	11.4432	0.1271	17.6193	11.4432
3	15.5470	0.1727	24.2627	15.5470
4	4.9792	0.0553	7.7045	4.9792
Total	37.8063	**0.4199**	58.6334	37.8063
Added mass (SbCl3) (g)		0.1843		

Solution 6	Oxalic Acid		Choline Chloride	
	mass (g)	moles	mass (g)	moles
1	25.0844	0.2786	38.6463	0.2768
2	12.7015	0.1411	25.4597	0.1823
3	3.5541	0.0395		
Total	41.3400	**0.4592**	64.1060	**0.4591**
Added mass (SbCl3) (g)		0.185		

Solution 7	Oxalic Acid		Choline Chloride	
	mass (g)	moles	mass (g)	moles
1	24.9385	0.2770	38.7992	0.2779
2	12.7770	0.1419	19.6903	0.1410
Total	37.7155	**0.4189**	58.4895	**0.4189**
Added mass (SbCl3) (g)		0.1813		

Solution 8	Oxalic Acid		Choline Chloride	
	mass (g)	moles	mass (g)	moles
1	5.9304	0.0659	9.0473	0.0648
2	10.2586	0.1139	15.7189	0.1126
3	15.1712	0.1685	23.7501	0.1701
4	6.4304	0.0714	10.1523	0.0727
Total	37.7906	**0.4198**	58.6686	**0.4202**
Added mass (SbCl3) (g)		0.1901		

Solution 9	Oxalic Acid		Choline Chloride	
	mass (g)	moles	mass (g)	moles
1	5.8803	0.0653	9.1952	0.0659
2	10.4458	0.1160	15.7855	0.1131
3	15.3151	0.1701	24.4140	0.1749

4	6.1769	0.0686	9.3405	0.0669
Total	37.8181	**0.4201**	58.7352	**0.4207**
Added mass (SbCl3) (g)		0.1845		

Solution 10	**Oxalic Acid**		**Choline Chloride**	
	mass (g)	moles	mass (g)	moles
1	5.0713	0.0563	7.8733	0.0564
2	10.0410	0.1115	15.8689	0.1137
3	10.5941	0.1177	16.2534	0.1164
4	12.4408	0.1382	19.1721	0.1373
Total	38.1472	**0.4237**	59.1677	**0.4238**
Added mass (SbCl3) (g)		0.1931		

Solution 11	**Oxalic Acid**		**Choline Chloride**	
	mass (g)	moles	mass (g)	moles
1	5.8281	0.0647	8.8139	0.0631
2	10.5507	0.1172	16.1657	0.1158
3	10.6272	0.1180	16.8710	0.1208
4	13.3856	0.1487	20.8074	0.1490
Total	40.3916	**0.4486**	62.6580	**0.4488**
Added mass (Sb2O3) (g)		0.2093		

Solution 12	**Oxalic Acid**		**Choline Chloride**	
	mass (g)	moles	mass (g)	moles
1	15.1677	0.1685	23.5572	0.1687
2	15.2676	0.1696	23.6565	0.1694
3	10.0886	0.1121	15.6408	0.1120
Total	40.5239	**0.4501**	62.8545	**0.4502**
Added mass (Sb2O3) (g)		0.1875		

Solution 13	**Oxalic Acid**		**Choline Chloride**	
	mass (g)	moles	mass (g)	moles
1	15.5655	0.1729	24.3745	0.1746
2	17.5714	0.1952	27.0238	0.1936
3	5.1211	0.0569	7.9367	0.0568
Total	38.2580	**0.4249**	59.3350	**0.4250**
Added mass (SbCl3) (g)		0.2093		

Solution 14	Oxalic Acid		Choline Chloride	
	mass (g)	moles	mass (g)	moles
1	5.9228	0.0658	9.2014	0.0659
2	9.8544	0.1095	15.1839	0.1088
3	9.7245	0.1080	15.2644	0.1093
4	13.4118	0.1490	20.6967	0.1482
Total	38.9135	**0.4322**	60.3464	**0.4322**
Added mass (SbCl3) (g)		0.193		

Solution 15	Oxalic Acid		Choline Chloride	
	mass (g)	moles	mass (g)	moles
1	6.7881	0.0754	10.5112	0.0753
2	9.9818	0.1109	15.4487	0.1106
3	10.0789	0.1120	15.6435	0.1120
4	12.0087	0.1334	18.6636	0.1337
Total	38.8575	**0.4316**	60.2670	**0.4317**
Added mass (SbCl3) (g)		0.1825		

Solution 16	Oxalic Acid		Choline Chloride	
	mass (g)	moles	mass (g)	moles
1	14.7328	0.1636	23.3898	0.1675
2	13.0243	0.1447	19.6548	0.1408
3	11.0075	0.1223	17.4813	0.1252
4	0.3346	0.0037	0.1770	0.0013
Total	39.0992	**0.4343**	60.7029	**0.4348**
Added mass (SbCl3) (g)		0.1883		

Solution 17	Oxalic Acid		Choline Chloride	
	mass (g)	moles	mass (g)	moles
1	13.5324	0.1503	21.6889	0.1553
2	13.1940	0.1466	20.6159	0.1477
3	14.1230	0.1569	21.1193	0.1513
4	0.0551	0.0006		
Total	40.9045	**0.4543**	63.4241	**0.4543**
Added mass (SbCl3) (g)		0.1857		

Solution 18	Oxalic Acid		Choline Chloride	
	mass (g)	moles	mass (g)	moles
1	13.7114	0.1523	21.3814	0.1531
2	13.5988	0.1510	20.9884	0.1503
3	13.6138	0.1512	21.0925	0.1511
Total	40.9240	**0.4546**	63.4623	**0.4545**
Added mass (SbCl3) (g)		0.1916		

Solution 19	Oxalic Acid		Choline Chloride	
	mass (g)	moles	mass (g)	moles
1	20.3642	0.2262	31.8157	0.2279
2	12.9654	0.1440	19.7814	0.1417
3	9.1525	0.1017	14.2946	0.1024
Total	42.4821	**0.4719**	65.8917	**0.4719**
Added mass (SbCl3) (g)		0.1938		

Solution 20	Oxalic Acid		Choline Chloride	
	mass (g)	moles	mass (g)	moles
1	6.0391	0.0671	9.4919	0.0680
2	7.9593	0.0884	12.1573	0.0871
3	12.4279	0.1380	19.5728	0.1402
4	13.8772	0.1541	21.2701	0.1523
Total	40.3035	**0.4477**	62.4921	**0.4476**
Added mass (SbCl3) (g)		0.1834		